IEEE Access
Multidisciplinary | Rapid Review | Open Access Journal

Received December 19, 2020, accepted January 5, 2021, date of publication January 11, 2021, date of current version January 20, 2021.

Digital Object Identifier 10.1109/ACCESS.2021.3050480

Rate-Energy Tradeoffs of Wireless Powered Backscatter Communication With Power Splitting and Time Switching

GERARDO SACARELO[1] AND YUN HEE KIM[1,2], (Senior Member, IEEE)
[1]Department of Electronics and Information Convergence Engineering, Kyung Hee University, Yongin 17104, South Korea
[2]Department of Electronic Engineering, Kyung Hee University, Yongin 17104, South Korea

Corresponding author: Yun Hee Kim (yheekim@khu.ac.kr)

This work was supported by the National Research Foundation of Korea (NRF) funded by the Korean Government (Ministry of Education) under Grant NRF-2018R1D1A1B07045515.

ABSTRACT We consider a monostatic wireless powered backscatter communication (WPBC) system, where a device performs backscatter modulation and energy harvesting (EH) using the received signal from a multi-antenna hybrid access point. The rate-energy regions of the WPBC are studied for power splitting (PS) and time switching (TS) receivers in a comprehensive way by using the rate and EH functions reflecting the effects of practical systems. For both linear and nonlinear EH models, we analyze the rate-energy regions of the static PS and TS strategies and optimize the dynamic strategies exploiting the channel state information (CSI) to extend the regions. The regions with the static strategies are obtained in closed-form expressions and the dynamic strategies are obtained in explicit forms as a function of a dual variable, by approximating the nonlinear EH model to a piecewise linear EH (PLEH) model. The results show that the dynamic PS and TS strategies outperform their static counterparts and their gains are more prominent in the sensitivity region of a nonlinear EH circuit and with a smaller number of antennas. It is also observed that the dynamic PS strategy provides the best performance but can be replaced by the static one for a large number of antennas to avoid the CSI. The strategies obtained explicitly by using the PLEH model are also shown to work well with a practical EH model without a noticeable loss in the performance.

INDEX TERMS Backscatter communication, nonlinear energy harvesting, power splitting, rate-energy region, time switching.

I. INTRODUCTION

The internet-of-things (IoT) is a key building block for smart society by connecting various objects that sense their environments and providing smart and autonomous controls using the sensed data. Diverse applications of the future IoT require sensing and communication devices to appear in various form factors, including small size devices that can be implementable with only a very small battery or even without a battery. As a method of enabling such devices sustainable for a long period, wireless power transfer (WPT) using radio frequency (RF) signals has been introduced into wireless communication protocols such as simultaneous wireless information and power transfer (SWIPT), wireless powered communication, wireless powered backscatter communication (WPBC) [1]–[4]. In particular, the WPBC is promising for power deficient devices by removing active modules for generating a carrier signal through backscatter modulation [3], [4].

Backscatter communication (BC) systems have been implemented in various configurations according to a source entity emitting a carrier signal and a destination receiving the backscatter signal for information decoding. Monostatic BC systems implement a source and a destination in the same entity [5], [6] while bistatic BC systems implement them in different entities [7]–[11]. Meanwhile, ambient BC systems utilize a transmitter of another services such as WiFi, cellular, and broadcasting ambient around backscatter devices as a source emitting the excitation signal [12]–[18].

This paper concerns with monostatic BC systems, where a full-duplex hybrid access point (HAP) transmits an excitation signal as well receives a backscatter signal

The associate editor coordinating the review of this manuscript and approving it for publication was Meng-Lin Ku.

simultaneously without self-interference [19]–[26]. Various aspects of monostatic BC systems have been investigated such as energy beamforming and channel estimation [19], [20], [23], throughput maximization for time division multiple access (TDMA) [21], multisine waveform designs with nonlinear energy harvesting [22], rate optimization for space division multiple access (SDMA) [24], [25], and space-time coding design for multi-antenna BC systems [26]. While most of these studies dealt with energy transfer problems [19], [20], [23] and rate transfer problems [24]–[26] separately, the studies in [21], [22] considered both the energy and rate transfer jointly for WPBC systems.

In monostatic WPBC systems using a common RF signal for energy harvesting (EH) and backscatter modulation (BM), there exists a fundamental trade-off between the harvested energy and delivered rate. Such trade-offs have been investigated extensively for the SWIPT, delivering the information and energy to a device in the same direction using a common RF signal, by means of the rate-energy region [27]–[33]. More specifically, the rate-energy regions of the SWIPT were investigated with linear EH circuits when time switching (TS) and power splitting (PS) receiver architectures supporting EH and information decoding (ID) simultaneously were implemented with the dynamic strategies adaptive to the channel state [27], [28] and the static ones [29]. Later, nonlinear EH models [34]–[36] were introduced to the SWIPT for a practical design, where the dynamic mode switching (MS) strategy selecting a mode between EH and ID was optimized in [30], [31], the static TS and PS strategies were considered for the optimization of a multi-sine waveform [32], and the dynamic PS strategy was optimized very recently in [33].

Rate-energy trade-offs in the WPBC have not been studied as much as those in the SWIPT since BM was limited to binary modulation schemes in the past. Hence, a trade-off of a monostatic WPBC system was investigated with the on-off binary BM in terms of the energy and signal-to-interference-and-noise ratio, where binary one was sent by reflecting the received signal fully and binary zero was presumed for no reflection [22]. Recent advances in the BM design enables high order quadrature amplitude modulation (QAM) [37]–[39], which makes the rate-energy region studied for the SWIPT also necessary for the WPBC to get an insight on the achievable performance.

This paper investigates the rate-energy regions achieved by monostatic WPBC systems under various configurations in the receiver architecture, availability of the channel sate information (CSI), nonlinearity of the EH function, and so on. The main contributions of this paper can be summarized as follows:

- We consider a point-to-point monostatic WPBC system with a multi-antenna HAP employing matched filter MF) beamforming and a backscatter device (BD) employing PS and TS receiver architectures. For the system, we provide a unified expression on the rate-energy region by adopting simple rate and energy functions incorporating the effect of a practical modulation scheme [40] and a practical EH circuit [35].
- The rate-energy regions of the WPBC achieved with the static factors for the PS and TS receiver architectures are derived in closed forms for both the linear and nonlinear EH models.
- The dynamic PS, MS, and TS strategies optimizing the rate-energy region of the WPBC are presented by solving the dual problem for both the linear and nonlinear EH models, where the dynamic MS strategy is shown to be equivalent to the dynamic TS strategy. The strategies optimized for the WPBC appear in more complicated forms when compared with those for the SWIPT [28], [30], [31], [33] but the optimization process in this paper is facilitated with a closed-form expression of the harvested energy for a given dual variable.
- The rate-energy regions of the WPBC are evaluated from various aspects with PS and TS receiver architectures, static and dynamic strategies, linear and non-linear EH functions, and Gaussian and practical modulation schemes. The rate-energy region behaviors are also investigated with the number of antennas in comparison with those of the SWIPT and those with a practical EH circuit.

The rest of this paper is organized as follows. Section II describes the system model and the rate-energy regions with different strategies. The rate-energy regions of the WPBC system are analyzed with the static strategies for PS and TS receiver architectures in Section III. Dynamic strategies adaptive to the channel state are optimized to extend the rate-energy region of the PS and TS receivers for the linear and nonlinear EH models in Section IV. The rate-energy regions of the WPBC systems are investigated under various configurations in Section V. Finally, concluding remarks are provided in Section VI.

Notation: $\mathbb{R}_+^n$ denotes the set of n-dimensional vectors with non-negative real-valued entries, $\mathbf{0}_m$ denotes the m-dimensional vector with all zero entries, and $\boldsymbol{I}_m$ denotes the $m \times m$ identity matrix. The complex Gaussian distribution with mean $\boldsymbol{\mu}$ and covariance $\boldsymbol{\Sigma}$ is denoted by $\mathcal{CN}(\boldsymbol{\mu}, \boldsymbol{\Sigma})$ and the expectation operation is denoted by $\mathbb{E}[\cdot]$.

II. SYSTEM MODEL AND RATE-ENERGY REGIONS

A. SYSTEM MODEL

Consider a monostatic WPBC system described in Fig. 1 that consists of a HAP equipped with M antennas and a single-antenna BD. The channel between the HAP and BD with path-loss ω is expressed as $\boldsymbol{h} = [h_1, h_2, \cdots, h_M]^T \sim \mathcal{CN}(\mathbf{0}_M, \omega \boldsymbol{I}_M)$ by assuming that the channels go through flat Rayleigh fading and the channel reciprocity holds. The HAP transmits an excitation signal as well as receives the backscatter signal in full-duplex as in [8], [19], [21]–[25].

The HAP employs the MF beamforming $\boldsymbol{w}_t = \frac{\boldsymbol{h}^*}{\|\boldsymbol{h}\|}$ to transmit the excitation signal at power P. The signal received at the BD antenna is then expressed as

$$y_B = \sqrt{P}\boldsymbol{h}^T \boldsymbol{w}_t + n_B = \sqrt{P}\|\boldsymbol{h}\| + n_B, \tag{1}$$

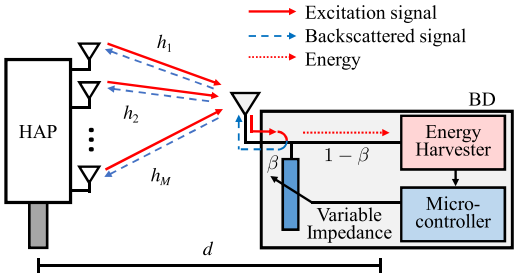

FIGURE 1. Monostatic WPBC with a multi-antenna HAP and a single-antenna BD.

where $n_B \sim \mathcal{CN}(0, \sigma_B^2)$ is the antenna noise at the BD. The BD splits the received signal (1) at power fractions β and $1-\beta$ for the BM and EH, respectively, as illustrated in Fig. 1. Note that $\beta \in \mathfrak{B}_P \triangleq [0, 1]$ is implementable only with the PS receiver supporting both BM and EH simultaneously while $\beta \in \mathfrak{B}_M \triangleq \{0, 1\}$ is implementable with the TS receiver supporting only one mode between BM and EH at a time.

The BM signal reflected by the BD is given by $s_B = \sqrt{\beta} y_B s$, where s is the modulation symbol generated by controlling the impedance load at the BD subject to $\mathbb{E}[|s|^2] = 1$. The BM signal received at the HAP is then expressed as

$$\boldsymbol{y} = \boldsymbol{h}\sqrt{\beta} y_B s + \boldsymbol{n} = \sqrt{P\beta}\boldsymbol{h}\|\boldsymbol{h}\| s + \sqrt{\beta}\boldsymbol{h} n_B s + \boldsymbol{n}, \quad (2)$$

where $\boldsymbol{n} \sim \mathcal{CN}(\boldsymbol{0}_M, \sigma^2 \boldsymbol{I}_M)$ is the additive Gaussian noise vector at the HAP. In practical backscattering scenarios, the power $\beta\|\boldsymbol{h}\|^2\sigma_B^2$ of the noise reflected by the BD is negligible compared with the power σ^2 of the noise $\boldsymbol{n}$ at the HAP due to the path loss. As in the literature [8], [21]–[25], the noise reflected by the BD is ignored as

$$\boldsymbol{y} \approx \sqrt{P\beta}\boldsymbol{h}\|\boldsymbol{h}\| s + \boldsymbol{n}. \quad (3)$$

The HAP detects symbol s by applying receive beamforming $\boldsymbol{w}_r$ to (3) as

$$z = \boldsymbol{w}_r^H \boldsymbol{y} = \sqrt{P\beta}\boldsymbol{w}_r^H \boldsymbol{h}\|\boldsymbol{h}\| s + \boldsymbol{w}_r^H \boldsymbol{n}. \quad (4)$$

The signal-to-noise ratio (SNR) in detecting the symbol is given by

$$\gamma = P\beta\|\boldsymbol{h}\|^2 \frac{\boldsymbol{w}_r^H \boldsymbol{h}\boldsymbol{h}^H \boldsymbol{w}_r}{\sigma^2 \boldsymbol{w}_r^H \boldsymbol{w}_r} \quad (5)$$

of which the maximum is achieved with MF beamforming $\boldsymbol{w}_r = c\boldsymbol{h}$ for any nonzero constant c [41] such that

$$\gamma = \frac{P\beta\|\boldsymbol{h}\|^4}{\sigma^2}. \quad (6)$$

Thus, the instantaneous rate delivered from the BD to the HAP for given channel $\boldsymbol{h}$ can be expressed as

$$R = C\left(\kappa \frac{P}{\sigma^2}\beta\|\boldsymbol{h}\|^4\right), \quad (7)$$

where $C(x) = \log_2(1 + x)$ and κ is the SNR loss incurred by employing a practical modulation scheme instead of Gaussian symbols; $\kappa = 1$ for Gaussian symbols and $\kappa \approx \frac{-1.5}{\ln(5\epsilon)}$ for the adaptive QAM employed at the bit error rate (BER) ϵ [40].

In the meantime, the signal $\sqrt{1-\beta} y_B$ at the BD is input to the energy harvester, where the EH from the noise is not considered as in [27]–[32] since the noise power $(1-\beta)\sigma_B^2$ is also negligible in comparison with the excitation signal power $P\|\boldsymbol{h}\|^2(1-\beta)$. The EH circuit of the BD harvests the energy with the instantaneous input power $p_{in} = P(1-\beta)\|\boldsymbol{h}\|^2$ for the use of essential operations such as sensing and chip processing. The harvested energy per unit time is expressed as

$$Q_{\mathfrak{h}} = \Phi_{\mathfrak{h}}(P(1-\beta)\|\boldsymbol{h}\|^2), \quad (8)$$

where $\Phi_{\mathfrak{h}}(\cdot)$ is the input-output power function of the EH circuit according to the EH model $\mathfrak{h}$.

For the EH, we consider the LEH model with EH efficiency η as

$$\Phi_L(p) = \eta p \quad (9)$$

and the NLEH model based on the piecewise linear EH (PLEH) developed in [34]–[36] as[1]

$$\Phi_N(p) = \begin{cases} 0, & \text{if } 0 \le p < p_a, \\ \eta(p - p_a), & \text{if } p_a \le p < p_b, \\ P_{sat}, & \text{if } p \ge p_b, \end{cases} \quad (10)$$

where p_a is the input power required to activate the EH circuit and p_b is the input power driving the EH circuit into the saturation region at saturation power P_{sat}. The PLEH function (10) approximates the sensitivity inclusive sigmoid EH (SSEH) function [34]

$$\Phi_S(p) = \begin{cases} 0, & \text{if } 0 \le p < p_a, \\ P_{sat}\dfrac{1 - e^{-\mu(p-p_a)}}{1 + e^{-\mu(p-p_c)}}, & \text{if } p \ge p_a \end{cases} \quad (11)$$

with the positive charging rate μ and the curvature point p_c, in a way of embracing the three crucial regions observed in practical EH circuits; the sensitivity region of $0 \le p < p_a$ where the EH circuit is inactive, the linear region of $p_a \le p < p_b$ with EH efficiency η, and the saturation region of $p \ge p_b$. Although the linear region can be partitioned into more pieces with different slopes for a better approximation of the EH function as in [35], we adopt the PLEH model (10) with three regions for a tractable analysis without a noticeable change in the rate-energy regions.

B. RATE-ENERGY REGIONS

Using the rate function (7) and the EH function (8), we consider the rate-energy regions of the WPBC with different strategies in choosing the PS factor according to the channel state[2] $X = \|\boldsymbol{h}\|^2$. the dynamic PS strategy chooses a different PS factor $\beta(X) \in \mathfrak{B}_P$ according to the channel state X while the static PS strategy sets $\beta = \bar{\beta}$ for all possible realizations

[1]The PLEH model is denoted by the subscript N to emphasize the nonlinearity while avoiding a confusion with the subscript P used for the PS strategy.

[2]The channel state $\|\boldsymbol{h}\|^2$ is denoted by X when it is interpreted as a random variable and by x when it is interpreted as a realization of the random variable.

of the channel state X. The dynamic MS strategy $\beta(X) \in \mathfrak{B}_M$ is a suboptimal approach of the dynamic PS strategy. We then rewrite the instantaneous rate with $\beta(X)$ as

$$R(\beta(X), X) = C\left(\gamma_0 \beta(X) X^2\right) \tag{12}$$

from (7) with the effective SNR $\gamma_0 = \kappa P/\sigma^2$ at the transmitter side and the instantaneous harvested energy with $\beta(X)$ as

$$Q_{\mathfrak{h}}(\beta(X), X) = \Phi_{\mathfrak{h}}(P(1-\beta(X))X) \tag{13}$$

from (8).

The rate-energy region of the WPBC for the dynamic PS or MS strategy $\{\beta(X), X \in \mathbb{R}_+\}$ can be expressed in a unified form as

$$C_{R-E}^{\mathfrak{s},D} \triangleq \bigcup_{\{\beta(X)\in\mathfrak{B}_{\mathfrak{s}}\}} \Big\{(r,q) \in \mathbb{R}_+^2 | r \le \mathbb{E}[R(\beta(X), X], \; q \le \mathbb{E}[Q_{\mathfrak{h}}(\beta(X), X)]\Big\} \tag{14}$$

for $\mathfrak{s} \in \{P, M\}$ and $\mathfrak{h} \in \{L, N\}$. With the static PS strategy setting $\beta(X) = \bar{\beta} \in [0,1]$ for all channel state X, the region (14) becomes

$$C_{R-E}^{P,S} = \bigcup_{\bar{\beta}\in[0,1]} \{(r,q) \in \mathbb{R}_+^2 | r \le \bar{R}(\bar{\beta}), q \le \bar{Q}_{\mathfrak{h}}(\bar{\beta})\} \tag{15}$$

with

$$\bar{R}(\bar{\beta}) \triangleq \mathbb{E}[R(\bar{\beta}, X)] = \mathbb{E}\left[C(\gamma_0 \bar{\beta} X^2)\right] \tag{16}$$

and

$$\bar{Q}_{\mathfrak{h}}(\bar{\beta}) \triangleq \mathbb{E}[Q(\bar{\beta}, X)] = \mathbb{E}[\Phi_{\mathfrak{h}}(P(1-\bar{\beta})X)]. \tag{17}$$

In comparison, we also consider the TS strategies that allocate a time fraction $\tau(X)$ of each channel state X for BM as $\beta(X) = 1$ and the other fraction $1-\tau(X)$ for EH as $\beta(X) = 0$. The dynamic TS strategy chooses a different TS factor $\tau(X) \in [0,1]$ according to the channel state X while the static TS strategy sets $\tau = \tilde{\tau}$ for all possible realizations of the channel state X. The rate-energy region of the WPBC with the dynamic TS strategy is expressed as

$$C_{R-E}^{T,D} \triangleq \bigcup_{\{\tau(X)\in[0,1]\}} \Big\{(r,q) \in \mathbb{R}_+^2 | r \le \mathbb{E}[\tau(X) R(1, X)], \; q \le \mathbb{E}[(1-\tau(X)) Q_{\mathfrak{h}}(0, X)]\Big\} \tag{18}$$

for $\mathfrak{h} \in \{L, N\}$. The region (18) with the static TS, $\tau(X) = \bar{\tau} \in [0,1]$ for all channel state X, is given by

$$C_{R-E}^{T,S} = \bigcup_{\bar{\tau}\in[0,1]} \{(r,q) \in \mathbb{R}_+^2 | r \le \bar{\tau}\bar{R}(1), \; q \le (1-\bar{\tau})\bar{Q}_{\mathfrak{h}}(0)\}. \tag{19}$$

III. RATE-ENERGY REGIONS WITH STATIC STRATEGIES

This section analyzes the rate-energy regions (15) and (19) with the static strategies for a baseline performance for which the closed-form expressions of (16) and (17) are obtained. The expectation in (16) and (17) is performed over the channel state $X = \|\boldsymbol{h}\|^2$ which is a gamma random variable with a shape parameter M and a scale parameter ω from $\boldsymbol{h} \sim \mathbb{CN}(\boldsymbol{0}_M, \omega \boldsymbol{I}_M)$ with the probability density function (pdf)

$$f_X(x) = \frac{x^{M-1}}{\Gamma(M)\omega^M} e^{-\frac{x}{\omega}}, \quad x \ge 0, \tag{20}$$

where $\Gamma(m) = \int_0^\infty t^{m-1} e^{-t} dt$.

We first express the average rate (16) as

$$\bar{R}(\bar{\beta}) = \int_0^\infty G_{2,2}^{1,2}\left(\begin{matrix}1,1\\1,0\end{matrix}\middle| \gamma_0 \bar{\beta} x^2\right) \frac{x^{M-1} e^{-\frac{x}{\omega}}}{\omega^M \Gamma(M) \ln 2} dx. \tag{21}$$

using $C(x) = \frac{1}{\ln 2}\ln(1+x)$ and the Meijer G-function [42], [43]

$$\ln(1+x) = G_{2,2}^{1,2}\left(\begin{matrix}1,1\\1,0\end{matrix}\middle| x\right). \tag{22}$$

We then have a closed-form expression of (21) as

$$\begin{aligned}\bar{R}(\bar{\beta}) &= \frac{1}{\varrho(\bar{\beta})} \int_0^\infty G_{2,2}^{1,2}\left(\begin{matrix}\frac{M+1}{2}, \frac{M+1}{2}\\ \frac{M+1}{2}, \frac{M-1}{2}\end{matrix}\middle| \gamma_0 \bar{\beta} x^2\right) e^{-\frac{x}{\omega}} dx \\ &= \frac{\omega}{\varrho(\bar{\beta})\sqrt{\pi}} G_{4,2}^{1,4}\left(\begin{matrix}0, \frac{1}{2}, \frac{M+1}{2}, \frac{M+1}{2}\\ \frac{M+1}{2}, \frac{M-1}{2}\end{matrix}\middle| 4\gamma_0 \bar{\beta} \omega^2\right)\end{aligned} \tag{23}$$

for $\varrho(\bar{\beta}) = \omega^M \Gamma(M) (\gamma_0 \bar{\beta})^{\frac{M-1}{2}} \ln 2$ from the properties [42]

$$x^\nu G_{p,q}^{m,n}\left(\begin{matrix}\boldsymbol{a}_p\\ \boldsymbol{b}_q\end{matrix}\middle| x\right) = G_{p,q}^{m,n}\left(\begin{matrix}\boldsymbol{a}_p + \nu\\ \boldsymbol{b}_q + \nu\end{matrix}\middle| x\right) \tag{24}$$

and

$$\int_0^\infty e^{-\frac{x}{\omega}} G_{p,q}^{m,n}\left(\begin{matrix}\boldsymbol{a}_p\\ \boldsymbol{b}_q\end{matrix}\middle| \rho x^2\right) dx = \frac{\omega}{\sqrt{\pi}} G_{p+2,q}^{m,n+2}\left(\begin{matrix}0, \frac{1}{2}, \boldsymbol{a}_p\\ \boldsymbol{b}_q\end{matrix}\middle| 4\rho\omega^2\right). \tag{25}$$

The average harvested energy (17) is also derived as

$$\bar{Q}_L(\bar{\beta}) = \eta P(1-\bar{\beta})\mathbb{E}[X] = \eta P(1-\bar{\beta}) M\omega \tag{26}$$

for the LEH (9) and

$$\bar{Q}_N(\bar{\beta}) = \eta P(1-\bar{\beta}) M\omega \left[\mathfrak{G}_{M+1}\left(\frac{x_{a,\bar{\beta}}}{\omega}, \frac{x_{b,\bar{\beta}}}{\omega}\right) - \frac{x_{a,\bar{\beta}}}{M\omega}\mathfrak{G}_M\left(\frac{x_{a,\bar{\beta}}}{\omega}, \frac{x_{b,\bar{\beta}}}{\omega}\right)\right] + P_{sat}\,\alpha\left(M, \frac{x_{b,\bar{\beta}}}{\omega}\right) \tag{27}$$

for the nonlinear PLEH (10), where

$$x_{v,\beta} = \frac{p_v}{P(1-\beta)} \tag{28}$$

for $v \in \{a, b\}$,

$$\alpha(m,x) = \frac{\Gamma(m,x)}{\Gamma(m)} \tag{29}$$

being the regularized Gamma function with $\Gamma(m,x) = \int_x^\infty t^{m-1} e^{-t} dt$ satisfying $\Gamma(m+1,x) = m\Gamma(m,x) + x^m e^{-x}$, and

$$\mathfrak{G}_m(x_1, x_2) = \alpha(m, x_1) - \alpha(m, x_2). \tag{30}$$

IV. RATE-ENERGY REGIONS WITH DYNAMIC STRATEGIES

A. DYNAMIC PS STRATEGY

This subsection derives the dynamic PS strategy that optimizes the rate-energy region (14) for $\mathfrak{s} = P$, that is, $\beta(X) \in \mathfrak{B}_P = [0, 1]$. The region is optimized by maximizing the average rate under the requirement of the average harvested energy Q as

$$\max_{\{\beta(X)\in\mathfrak{B}_P\}} \mathbb{E}[R(\beta(X), X)] \tag{31a}$$

$$\text{s.t. } \mathbb{E}[Q_\mathfrak{h}(\beta(X), X)] \geq \mathsf{Q} \tag{31b}$$

for $0 \leq \mathsf{Q} \leq \bar{Q}_\mathfrak{h}(0)$, where $\mathfrak{h} \in \{L, N\}$. The average rate in the objective function given by

$$\mathbb{E}[R(\beta(X), X)] = \int_0^\infty C(\gamma_0\beta(x)x^2) f_X(x)dx \tag{32}$$

is concave for $\{\beta(x) \in [0, 1], x \in \mathbb{R}_+\}$ from $C(z) = \log_2(1+z)$, where $\{\beta(x) \in [0, 1], x \in \mathbb{R}_+\}$ can be interpreted as a vector $\boldsymbol{\beta}$ of an infinite length. The average harvested energy in the constraint (31b) is given by

$$\mathbb{E}[Q_\mathfrak{h}(\beta(X), X)] = \int_0^\infty \Phi_\mathfrak{h}(Px(1-\beta(x)))f_X(x)dx \tag{33}$$

so that the constraint with $\mathfrak{h} = L$ is linear for $\{\beta(x) \in [0, 1], x \in \mathbb{R}_+\}$. The constraint with $\mathfrak{h} = N$ is quasi-convex for $\{\beta(x) \in [0, 1], x \in \mathbb{R}_+\}$ since $\Phi_N(p)$ is a non-decreasing function of p. Thus, the primal problem (31) for the dynamic PS strategy satisfies the time sharing condition defined in [44] that guarantees a zero duality gap for both cases of LEH and nonlinear PLEH.

Thus, we solve the problem (31) through dual optimization as in [28], [30], [31] by forming the Lagrangian

$$\begin{aligned} L_{P,\mathfrak{h}}(\{\beta(X)\}, \lambda) &= \mathbb{E}[R(\beta(X), X)] \\ &\quad +\lambda(\mathbb{E}[Q_\mathfrak{h}(\beta(X), X)] - \mathsf{Q}) \\ &= \int_0^\infty l_{P,\mathfrak{h}}(\beta(x), \lambda, x) f_X(x)dx, \end{aligned} \tag{34}$$

where $\lambda \geq 0$ is the Lagrangian dual variable and

$$l_{P,\mathfrak{h}}(\beta, \lambda, x) = C(\gamma_0\beta x^2) + \lambda\{\Phi_\mathfrak{h}(P(1-\beta)x) - \mathsf{Q}\}. \tag{35}$$

The Lagrangian dual function for the PS strategy is then given by

$$g_{P,\mathfrak{h}}(\lambda) = \max_{\{\beta(X)\in\mathfrak{B}_P\}} L_{P,\mathfrak{h}}(\{\beta(X)\}, \lambda) \tag{36}$$

with the optimal PS strategy

$$\beta_{P,\mathfrak{h}}(x|\lambda) = \arg\max_{\beta\in\mathfrak{B}_P} l_{P,\mathfrak{h}}(\beta, \lambda, x) \tag{37}$$

for given $\lambda \in \mathbb{R}_+$ and $x \in \mathbb{R}_+$.

The optimal dual variable $\lambda^\star_{P,\mathfrak{h}} = \arg\min_{\lambda\geq 0} g_{P,\mathfrak{h}}(\lambda)$ for $\mathfrak{h} \in \{L, N\}$ is found by searching the value satisfying

$$\bar{Q}_{P,\mathfrak{h}|\lambda} \triangleq \mathbb{E}[\Phi_\mathfrak{h}(P(1-\beta_{P,\mathfrak{h}}(x|\lambda))x)] = \mathsf{Q} \tag{38}$$

from the complementary slackness [45]. The optimal dynamic strategy is then obtained with $\lambda^\star_{P,\mathfrak{h}}$ as

$$\beta^\star_{P,\mathfrak{h}}(x) = \beta_{P,\mathfrak{h}}(x|\lambda^\star_{P,\mathfrak{h}}) \tag{39}$$

for $\mathfrak{h} \in \{L, N\}$.

In the following theorems, we derive more explicit expressions of (37) for the LEH and PLEH by using the notation

$$\mathfrak{B}_q = \{x^2 - \varphi_q x + \frac{1}{\gamma_0} \geq 0\} \tag{40}$$

$$= \begin{cases} \{x < t_{q,1} \text{ or } x > t_{q,2}\} & \text{if } \varphi_q^2 > \dfrac{4}{\gamma_0} \\ \phi & \text{if } \varphi_q^2 \leq \dfrac{4}{\gamma_0} \end{cases} \tag{41}$$

for a set associated with a positive function φ_q identified by the subscript q, where

$$t_{q,1} = \frac{1}{2}\varphi_q - \sqrt{\frac{1}{4}\varphi_q^2 - \frac{1}{\gamma_0}},\ t_{q,2} = \frac{1}{2}\varphi_q + \sqrt{\frac{1}{4}\varphi_q^2 - \frac{1}{\gamma_0}}. \tag{42}$$

Theorem 1: The dynamic PS strategy (37) *for the LEH* (9) *is expressed as*

$$\beta_{P,L}(x|\lambda) = \begin{cases} 0 & \text{if } x < x_0, \\ \dfrac{1}{\gamma_0 x^2}\left(\frac{x}{x_0} - 1\right) & \\ & \text{if } x_0 < x < t_{0,1} \text{ or } x > t_{0,2}, \\ 1 & \text{if } t_{0,1} \leq x \leq t_{0,2} \end{cases} \tag{43}$$

for $\lambda < \frac{1}{2}\lambda_{\text{ip}}$ *with* $\lambda_{\text{ip}} = \frac{\sqrt{\gamma_0}}{\eta P \ln 2}$ *while*

$$\beta_{P,L}(x|\lambda) = \begin{cases} 0 & \text{if } x < x_0, \\ \dfrac{1}{\gamma_0 x^2}\left(\dfrac{x}{x_0} - 1\right) & \text{if } x \geq x_0 \end{cases} \tag{44}$$

for $\lambda \geq \frac{1}{2}\lambda_{\text{ip}}$, *where* $x_0 = \lambda\frac{\eta P \ln 2}{\gamma_0}$ *and* $\{t_{0,i}\}_{i=1}^2$ *are given by* (42) *with* $\varphi_0 = \frac{1}{x_0\gamma_0}$.[3]

Proof: See Appendix A-A. □

Remark: In Theorem 1, λ_{ip} is the value of λ leading to $x_0 = \frac{1}{\sqrt{\gamma_0}}$ which is the inflection point of the rate function $C(\gamma_0 x^2)$ leading to $\frac{\partial^2}{\partial x^2}C(\gamma_0 x^2) = 0$.

Theorem 2 (): The dynamic PS strategy (37) *for the nonlinear PLEH* (10) *at given dual variable* λ *is expressed as* (45), *as shown at the bottom of the next page,*[4] *where* $x_v = p_v/P$ *for* $v \in \{a, b\}$,

$$D_{N2}(x|\lambda) = C(\gamma_0 x^2) - \lambda\eta P(x - x_a), \tag{46}$$

$t_{b,2}$ *is expressed as* (42) *with* $\varphi_b = x_b + \frac{1}{\gamma_0 x_0}$, *and* $\mathfrak{B}_w$ *is expressed as* (40) *with*

$$\varphi_w = -\frac{1}{\gamma_0 x_0} W_{-1}(-e^{-x_0\gamma_0 x_a - 1}) \tag{47}$$

for the Lambert W function $W_k(\cdot)$ *[46].*

[3] In (43) and (44), x_0, $t_{0,1}$, and $t_{0,2}$ are functions of λ but the argument λ is omitted for the simplicity in the notation.

[4] We assume that $x_b > \frac{2}{\sqrt{\gamma_0}}$ since $x_b \approx 10^{-3}$ and $\gamma_0 \gg 10^8$ in practice.

Proof: See Appendix A-B. □

$$\bar{Q}_{P,L|\lambda} = \eta P M \omega \left\{1 - \mathfrak{G}_{M+1}(\frac{t_{0,2}}{\omega}, \frac{t_{0,1}}{\omega})\right\} - \frac{\eta P}{\gamma_0 x_0}\left\{\mathfrak{G}_M(\frac{x_0}{\omega}, \frac{t_{0,1}}{\omega}) + \alpha(M, \frac{t_{0,2}}{\omega})\right\} + \frac{\eta P}{\gamma_0 \omega}\left\{I_{M-1}(\frac{x_0}{\omega}) - I_{M-1}(\frac{t_{0,1}}{\omega}) + I_{M-1}(\frac{t_{0,2}}{\omega})\right\} \tag{48}$$

$$\bar{Q}_{P,N|\lambda} = \eta P M \omega \mathfrak{G}_{M+1}(\frac{t_{w,2}}{\omega}, \frac{t_{b,2}}{\omega}) + \eta P x_b \alpha(M, \frac{t_{b,2}}{\omega}) - \frac{\eta P}{\gamma_0 x_0}\mathfrak{G}_M(\frac{t_{w,2}}{\omega}, \frac{t_{b,2}}{\omega}) + \frac{\eta P}{\gamma_0 \omega}\{I_{M-1}(\frac{t_{w,2}}{\omega}) - I_{M-1}(\frac{t_{b,2}}{\omega})\}. \tag{49}$$

Lemma 1: If $x_a > \frac{1}{\sqrt{\gamma_0}}$, (45) *for* $0 < \lambda < \frac{1}{2}\lambda_{\text{ip}}$ *is given by*

$$\beta_{P,N}(x|\lambda) = \begin{cases} 1 & \text{if } x < t_{w,2}, \\ \frac{1}{\gamma_0 x^2}\left(\frac{x}{x_0} - 1\right) & \text{if } t_{w,2} \le x \le t_{b,2}, \\ 1 - \frac{x_b}{x} & \text{if } x > t_{b,2}, \end{cases} \tag{50}$$

where $t_{w,2}$ *is expressed as* (42) *with* (47).

Proof: See Appendix A-C. □

The average harvested energy is then derived as (48) with the dynamic PS factor (43) for the LEH and as (49) with the dynamic PS factor (50) for the PLEH, where $I_0(x) = -\text{Ei}(-x) = -\int_x^\infty \frac{1}{u}e^{-u}du$ and $I_m(x) = \frac{\Gamma(m)}{\Gamma(m+1)}\alpha(m, x)$ for $m > 0$. The average harvested energy with the dynamic PS factor (44) for the LEH is obtained as (43) with $t_{0,1} = t_{0,2} = \infty$.

B. DYNAMIC MS STRATEGY

This subsection derives the dynamic MS strategy that optimizes the rate-energy region (14) for $\mathfrak{s} = M$, that is, $\beta(X) \in \mathfrak{B}_M = \{0, 1\}$. The strategy is obtained by solving

$$\max_{\{\beta(X)\in\mathfrak{B}_M\}} \mathbb{E}[R(\beta(X), X)] \tag{51a}$$

$$\text{s.t. } \mathbb{E}[Q_{\mathfrak{h}}(\beta(X), X)] \ge \mathsf{Q} \tag{51b}$$

for $0 \le \mathsf{Q} \le \bar{Q}_{\mathfrak{h}}(0)$ and $\mathfrak{h} \in \{L, N\}$. The problem (51), which is almost the same with the problem (31) except for $\beta(X) \in \mathfrak{B}_M$, also satisfies the time sharing condition that guarantees a zero duality gap from the same reasoning provided in [31]. Thus, we can solve the problem (51) through dual optimization by following the approaches applied for the problem with the dynamic PS strategy.

In brief, the Lagrangian dual function for the dynamic MS strategy is given by

$$g_{M,\mathfrak{h}}(\lambda) = \max_{\{\beta(X)\in\mathfrak{B}_M\}} L_{P,\mathfrak{h}}(\{\beta(X)\}, \lambda) \tag{52}$$

with the optimal MS strategy

$$\beta_{M,\mathfrak{h}}(x|\lambda) = \arg\max_{\beta\in\mathfrak{B}_M} l_{P,\mathfrak{h}}(\beta, \lambda, x) \tag{53}$$

for given $\lambda \in \mathbb{R}_+$ and $x \in \mathbb{R}_+$, where $\mathfrak{h} \in \{L, N\}$. Note that $L_{P,\mathfrak{h}}(\{\beta(X)\}, \lambda)$ and $l_{P,\mathfrak{h}}(\beta, \lambda, x)$ are the functions used for the dynamic PS strategy defined in (34) and (35), respectively. Since there exist only two candidates for the optimal MS strategy, the optimal MS strategy is obtained as

$$\beta_{M,\mathfrak{h}}(x|\lambda) = \begin{cases} 1 & \text{if } D_{\mathfrak{h}}(x|\lambda) > 0 \\ 0 & \text{if } D_{\mathfrak{h}}(x|\lambda) < 0, \end{cases} \tag{54}$$

where $D_{\mathfrak{h}}(x|\lambda) = l_{P,\mathfrak{h}}(1, \lambda, x) - l_{P,\mathfrak{h}}(0, \lambda, x)$ is given by

$$D_{\mathfrak{h}}(x|\lambda) = C(\gamma_0 x^2) - \lambda\Phi_{\mathfrak{h}}(Px). \tag{55}$$

The following theorems provide more explicit expressions for the optimal MS strategy (54) with the LEH and PLEH, respectively.

Theorem 3: The dynamic MS strategy (54) *for the LEH* (9) *is expressed as*

$$\beta_{M,L}(x|\lambda) = \begin{cases} 1 & \text{if } z_{L,1} \le x \le z_{L,2},\ 0 < \lambda < \lambda_{\text{ip}}\sqrt{\breve{z}}, \\ 0 & \text{otherwise} \end{cases} \tag{56}$$

where $z_{L,1}$ *and* $z_{L,2}$ *are the zeros of* $D_L(x|\lambda)$ *for* $x > 0$ *and* $\breve{z} \approx 0.6476$ *is the zero of*

$$g(y) = \ln\left(\frac{2}{y}(1 + \sqrt{1-y})\right) - 1 - \sqrt{1-y} \tag{57}$$

for $y \in [0, 1]$.

Proof: See Appendix B-A. □

Theorem 4: The dynamic MS strategy (54) *for the nonlinear PLEH* (10) *is given as in Table 1 according to* N_z *zeros* $\{z_{N,i}\}_{i=1}^{N_z}$ *of* $D_{N2}(x|\lambda)$ *found in* $x_a \le x < x_b$, *where* $\lambda_s = \frac{C(\gamma_0 x_b^2)}{P_{sat}}$ *and* $z_S = \frac{\sqrt{2^{\lambda P_{sat}} - 1}}{\sqrt{\gamma_0}}$.

Proof: See Appendix B-B. □

Lemma 2: If $x_a > \frac{1}{\sqrt{\gamma_0}}$, *a non-trivial dynamic TS solution exists only when* $\lambda \ge \lambda_s$.

Proof: See Appendix B-C. □

$$\beta_{P,N}(x|\lambda) = \begin{cases} 0 & \text{if } x \in \tilde{\mathfrak{X}}_0 \triangleq \{x < x_0, x_a \le x < x_b, D_{N2}(x|\lambda) \le 0\}, \\ \frac{1}{\gamma_0 x^2}\left(\frac{x}{x_0} - 1\right) & \text{if } x \in \tilde{\mathfrak{X}}_z \triangleq \{\{\max(x_0, x_a) \le x < \max(x_b, t_{b,2})\} \cap \mathfrak{B}_w\} \\ 1 - \frac{x_b}{x} & \text{if } x \in \tilde{\mathfrak{X}}_b \triangleq \{x \ge \max(x_b, t_{b,2})\}, \\ 1 & \text{otherwise}, \end{cases} \tag{45}$$

TABLE 1. Dynamic MS strategy and average harvested energy for given dual variable.

Dual variable λ	N_z	Dynamic MS strategy	Average harvested energy
$0<\lambda<\lambda_s$	$N_z=2$	$\beta_{M,N}(x\|\lambda)=\begin{cases}1 & \text{if } x<z_{N,1} \text{ or } x>z_{N,2},\\ 0 & \text{if } z_{N,1}\le x<z_{N,2}\end{cases}$	$\bar{Q}_{M,N\|\lambda}=\eta PM\omega\mathfrak{G}_{M+1}\left(\frac{z_{N,1}}{\omega},\frac{z_{N,2}}{\omega}\right)$
$\lambda_s\le\lambda<\lambda_{\text{ip}}$	$N_z=3$	$\beta_{M,N}(x\|\lambda)=\begin{cases}1 & \text{if } x<z_{N,1} \text{ or } z_{N,2}<x<z_{N,3} \text{ or } x>z_S,\\ 0 & \text{if } z_{N,1}<x<z_{N,2} \text{ or } z_{N,3}<x<z_S\end{cases}$	$\bar{Q}_{M,N\|\lambda}=\eta PM\omega\mathfrak{G}_{M+1}\left(\frac{z_{N,1}}{\omega},\frac{z_{N,2}}{\omega}\right)+\eta PM\omega\mathfrak{G}_{M+1}\left(\frac{z_{N,3}}{\omega},\frac{x_b}{\omega}\right)+P_{\text{sat}}\mathfrak{G}_M\left(\frac{x_b}{\omega},\frac{z_S}{\omega}\right)$
$\lambda\ge\lambda_s$	$N_z=1$	$\beta_{M,N}(x\|\lambda)=\begin{cases}1 & \text{if } x<z_{N,1} \text{ or } x>z_S,\\ 0 & \text{if } z_{N,1}\le x<z_S\end{cases}$	$\bar{Q}_{M,N\|\lambda}=\eta PM\omega\mathfrak{G}_{M+1}\left(\frac{z_{N,1}}{\omega},\frac{x_b}{\omega}\right)+P_{\text{sat}}\mathfrak{G}_M\left(\frac{x_b}{\omega},\frac{z_S}{\omega}\right)$
$0<\lambda<\infty$	$N_z=0$	$\beta_{M,N}(x\|\lambda)=1$	$Q_{M,N\|\lambda}=0$

The average harvested energy with the dynamic MS strategy (56) is given as

$$\bar{Q}_{M,L|\lambda}=\frac{\eta P\omega}{\Gamma(M)}\mathfrak{G}_{M+1}\left(\frac{z_{L,1}}{\omega},\frac{z_{L,2}}{\omega}\right) \tag{58}$$

for the LEH and as Table 1 for the PLEH. For the LEH, the optimal dual variable is found in $0<\lambda<\lambda_{\text{ip}}\sqrt{\xi}$ since the average harvested energy is the maximum value $\bar{Q}_{M,L|\lambda}=\bar{Q}_L(0)$ with the trivial solution $\beta_{M,L}(x|\lambda)=0$ if $\lambda\ge\lambda_{\text{ip}}\sqrt{\xi}$.

The optimal dual variable $\lambda^\star_{M,\mathfrak{h}}=\arg\min_{\lambda\ge0} g_{M,\mathfrak{h}}(\lambda)$ of the dynamic MS strategy for $\mathfrak{h}\in\{L,N\}$ is found as in the dynamic PS strategy by searching the value satisfying

$$\bar{Q}_{M,\mathfrak{h}|\lambda}\triangleq\mathbb{E}[\Phi_{\mathfrak{h}}(P(1-\beta_{M,\mathfrak{h}}(x|\lambda))x)]=\mathsf{Q} \tag{59}$$

using (58) and Table 1, which leads to the optimal MS strategy $\beta^\star_{M,\mathfrak{h}}(x)=\beta_{M,\mathfrak{h}}(x|\lambda^\star_{M,\mathfrak{h}})$ for $\mathfrak{h}\in\{L,N\}$.

C. DYNAMIC TS STRATEGY

The dynamic TS strategy that optimizes the rate-energy region (18) is obtained by solving

$$\max_{\{\tau(X)\in[0,1]\}}\ \mathbb{E}[\tau(X)R(1,X)] \tag{60a}$$

$$\text{s.t. } \mathbb{E}[(1-\tau(X))Q_{\mathfrak{h}}(0,X)]\ge\mathsf{Q}, \tag{60b}$$

which is a linear program with respect to $\{\tau(x)\in[0,1], x\in\mathbb{R}_+\}$. Thus, the optimal solution of (60) is obtained with the Lagrangian dual optimization again. The Lagrangian of (60) is expressed as

$$L_{T,\mathfrak{h}}(\{\tau(X)\},\lambda)=\int_0^\infty l_{T,\mathfrak{h}}(\tau(x),\lambda,x)f_X(x)dx \tag{61}$$

with

$$l_{T,\mathfrak{h}}(\tau,\lambda,x)=\tau C(\gamma_0x^2)+\lambda\{(1-\tau)\Phi_{\mathfrak{h}}(Px)-\mathsf{Q}\} \tag{62}$$

for $\mathfrak{h}\in\{L,N\}$. The optimal TS allocation maximizing the Lagrangian dual function is achieved with

$$\tau_{\mathfrak{h}}(x|\lambda)=\arg\max_{\tau\in[0,1]} l_{T,\mathfrak{h}}(\tau,\lambda,x) \tag{63}$$

for given λ and $x\in\mathbb{R}_+$, where

$$l_{T,\mathfrak{h}}(\tau,\lambda,x)=\tau D_{\mathfrak{h}}(x|\lambda)+\lambda\{\Phi_{\mathfrak{h}}(Px)-\mathsf{Q}\} \tag{64}$$

with $D_{\mathfrak{h}}(x|\lambda)=C(\gamma_0x^2)-\lambda\Phi_{\mathfrak{h}}(Px)$ defined in (55). Since $l_{T,\mathfrak{h}}(\tau,\lambda,x)$ is a linear function of τ, it is immediate that

$$\tau_{\mathfrak{h}}(x|\lambda)=\begin{cases}1 & \text{if } D_{\mathfrak{h}}(x|\lambda)>0\\ 0 & \text{if } D_{\mathfrak{h}}(x|\lambda)<0.\end{cases} \tag{65}$$

Note that the dynamic TS strategy allocates BM as $\beta=1$ for $\tau_{\mathfrak{h}}(x|\lambda)$ and EH as $\beta=0$ for $1-\tau_{\mathfrak{h}}(x|\lambda)$, which implies that the optimal dynamic TS strategy (65) is equivalent to the dynamic MS strategy provided in (54). Thus, the dynamic TS strategies for the LEH and nonlinear PLEH are equivalent to the dynamic MS strategies provided in Theorems 3 and 4, respectively, by replacing $\beta_{\mathfrak{h}}(x|\lambda)$ with $\tau_{\mathfrak{h}}(x|\lambda)$ for $\mathfrak{h}\in\{L,N\}$. Thus, the optimal dual variable $\lambda^\star_{T,\mathfrak{h}}=\arg\min_{\lambda\ge0} g_{T,\mathfrak{h}}(\lambda)$ of the dynamic TS strategy for $\mathfrak{h}\in\{L,N\}$ is also identical to $\lambda^\star_{M,\mathfrak{h}}$ of the dynamic MS strategy and hence the optimal dynamic TS strategy is also given by $\tau^\star_{\mathfrak{h}}(x)=\beta^\star_{M,\mathfrak{h}}(x)$.

Remark: We would like to mention that the optimal dual variable $\lambda^\star_{\mathfrak{s},\mathfrak{h}}$ for each strategy $\mathfrak{s}$ and EH model $\mathfrak{h}$ can be found more efficiently by using the average harvested energy derived for given λ. Once $\lambda^\star_{\mathfrak{s},\mathfrak{h}}$ is found, the optimal factor of the method is straightforward from Theorems 1-4.

V. PERFORMANCE EVALUATION

This section investigates the average rate-energy regions of the WPBC system under various configurations by using $\eta=0.5734$ for the LEH (9) and using $\eta=0.5918$, $p_a=64$ μW, $p_b=8.389$ mW, and $P_{sat}=4.927$ mW for the NLEH based on the PLEH (10) developed to approximate the SSEH function with $\mu=274$, $p_c=1.058\times10^{-3}$, and $p_a=64$ μW employed in [34], [36]. We set the transmit power of the HAP to $P=3$ W, noise power of the HAP to $\sigma^2=-80$ dBm, and path-loss at distance d to $\omega=0.001d^{-2.5}$. Simulation results are obtained with 10^6 channel realizations for each point.

A. PERFORMANCES WITH DIFFERENT STRATEGIES

This subsection validates the static and dynamic strategies derived for the WPBC system by investigating their rate-energy regions through analysis and simulation. We investigate the rate-energy regions of the system with the adaptive QAM at BER $\epsilon=10^{-3}$ resulting in $\kappa=0.28$ for the LEH model (9) and nonlinear PLEH model (10); different

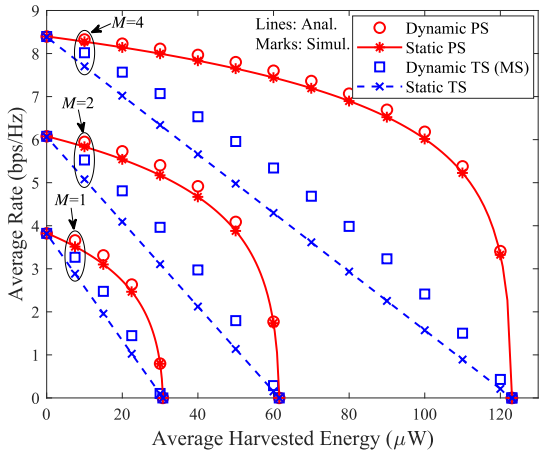

FIGURE 2. Rate-energy regions of the WPBC with the LEH when $d = 5$ m, $M = 1, 2, 4$, and the adaptive QAM at BER $\epsilon = 10^{-3}$ is employed.

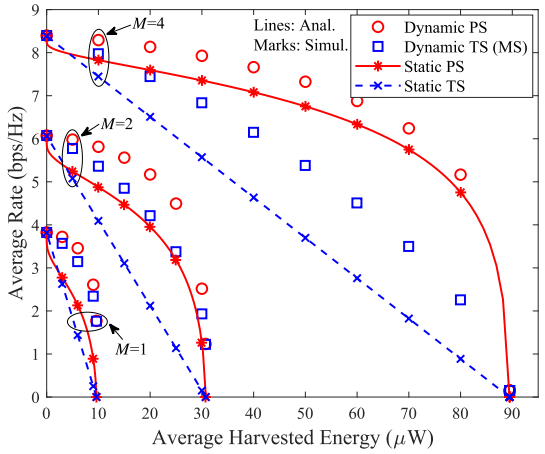

FIGURE 3. Rate-energy regions of the WPBC with the PLEH when $d = 5$ m, $M = 1, 2, 4$, and the adaptive QAM at BER $\epsilon = 10^{-3}$ is employed.

ranges of the input power for the PLEH is considered by varying the number of antennas and the distance of the BD. Since the dynamic MS strategy is equivalent to the dynamic TS strategy, we compare the performances of the PS and TS strategies mostly herein.

Figs. 2 and 3 show the rate-energy regions with various strategies when $d = 5$ m and the number of antennas varies as $M = 1, 2$, and 4. The LEH and PLEH models are employed in Figs. 2 and 3, respectively, where the results from both simulation (denoted by 'Simul.') and analysis (denoted by 'Anal.') are provided for the static strategies while the results from simulation are provided for the dynamic ones. It is confirmed that the results from analysis agree with those from simulation and the dynamic PS (TS) strategy outperforms its static counterpart by exploiting the CSI. In addition, the rate-energy region gets larger as M increases and the best performance is achieved with the dynamic PS. In case of the LEH, the dynamic PS, static PS, dynamic TS, and static TS are the order of performance for given M, which indicates that the receiver architecture rather than the CSI dominates the performance. In case of the PLEH, the dynamic

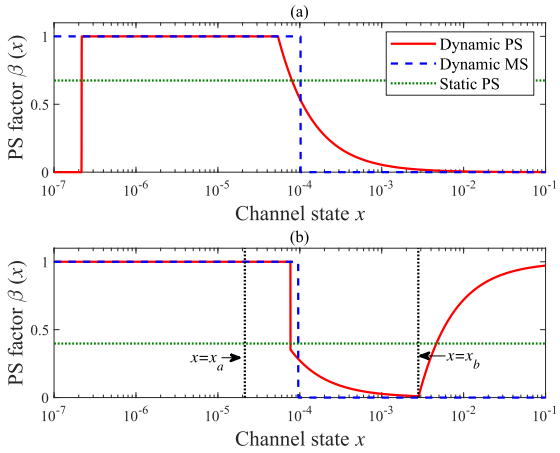

FIGURE 4. Dynamic PS and MS factors for (a) LEH and (b) PLEH when $d = 5$ m, $M = 4$, and $\mathsf{Q} = 40$ μW.

TS outperforms the static PS for a smaller number of antennas as $M = 1$ and 2, where a larger variation of the channel fading increases the probability of the PLEH circuit operating in the sensitivity region. If the EH circuit encounters the sensitivity region more often, the dynamic TS choosing one mode tends to be more preferable than the static PS splitting the received signal for BM and EH always.

The optimal dynamic PS factor $\beta^{\star}_{P,\mathfrak{h}}(x)$ and optimal dynamic MS factor $\beta^{\star}_{M,\mathfrak{h}}(x)$ (equivalent to the dynamic TS factor $\tau^{\star}_{\mathfrak{h}}(x)$) providing the results of Figs. 2 and 3 for $M = 4$ and $\mathsf{Q} = 40$ μW are shown as a function of the channel state x in Fig. 4(a) for $\mathfrak{h} = L$ and in Fig. 4(b) for $\mathfrak{h} = N$. The static PS factor $\bar{\beta}$ is also shown as a benchmark, and $x_a = 2.1 \times 10^{-5}$ and $x_b = 2.8 \times 10^{-3}$ are specified for the PLEH. In the figures, $\gamma_0 = 8.5 \times 10^{10}$, which leads to $\lambda^{\star}_{P,L} = 1.5 \times 10^4$, $\lambda^{\star}_{M,L}(\lambda^{\star}_{T,L}) = 5.1 \times 10^6$, $\lambda^{\star}_{P,N} = 3.0 \times 10^4$, and $\lambda^{\star}_{M,L}(\lambda^{\star}_{T,N}) = 5.9 \times 10^6$. In the case, $\beta^{\star}_{P,L}(x)$ is given by (43) with $x_0 \approx t_{0,1} = 2.2 \times 10^{-7}$ and $t_{0,2} = 5.4 \times 10^{-5}$, and $\beta^{\star}_{M,L}(x)$ is given by (56) with $z_{L,1} = 4.4 \times 10^{-18}$ and $z_{L,2} = 1.0 \times 10^{-4}$ in Fig. 4(a), where $z_{L,1}$ is out of the range. In the meantime, since $x_a > \frac{1}{\sqrt{\gamma_0}}$ for the PLEH, $\beta^{\star}_{P,N}(x)$ is given by (45) from Lemma 1 and $\beta^{\star}_{M,N}(x)$ is given by $\beta_{M,N}(x|\lambda)$ for $\lambda \geq \lambda_s$ and $N_z = 1$ in Table 1 from Lemma 2, where $t_{w,2} = 7.7 \times 10^{-5}$, $t_{b,2} = 2.8 \times 10^{-3}$, $z_{N,1} = 9.6 \times 10^{-5}$, and $z_S \gg 1$. The dynamic MS (TS) strategies behaves similar for the LEH and PLEH since the average channel power, $E[X] = M\omega = 7.2 \times 10^{-5}$, is in the region of the BM being preferred than the EH.

To identify a performance tendency with the PLEH operating around the saturation region, we consider a closer distance as $d = 2$ m and a larger number antennas as $M = 8, 16, 32$ in obtaining the rate-energy regions in Fig. 5. The gain of the dynamic TS over the static TS is reduced as M increases due to the reduced fading fluctuation. In the meantime, the rate-energy regions of the PS strategies are almost indistinguishable and get close to the upper-bound formed by the maximum rate $\bar{R}(1)$ and energy $\bar{Q}_N(0)$ as M increases since the fading fluctuation is reduced significantly.

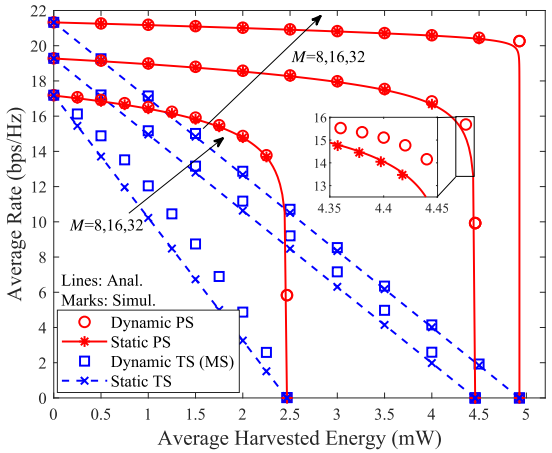

FIGURE 5. Rate-energy regions of the WPBC with the PLEH when $d = 2$ m, $M = 8$, 16, 32, and the adaptive QAM at BER 10^{-3} is employed.

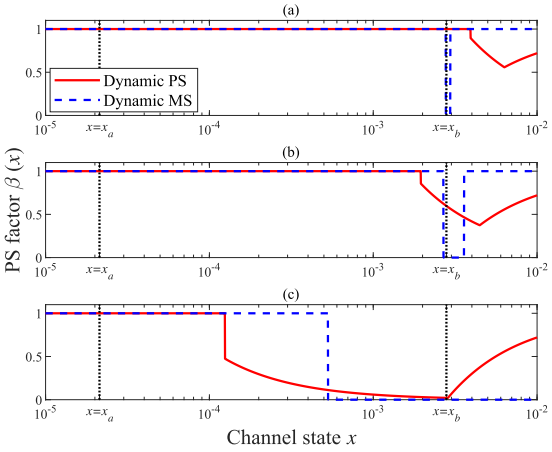

FIGURE 6. Dynamic PS and MS factors of the WPBC with the PLEH when $d = 2$ m, $M = 16$, and the adaptive QAM at BER 10^{-3} is employed: (a) Q = 0.1 mW, (b) Q = 2.0 mW, and (c) Q = 4.4 mW.

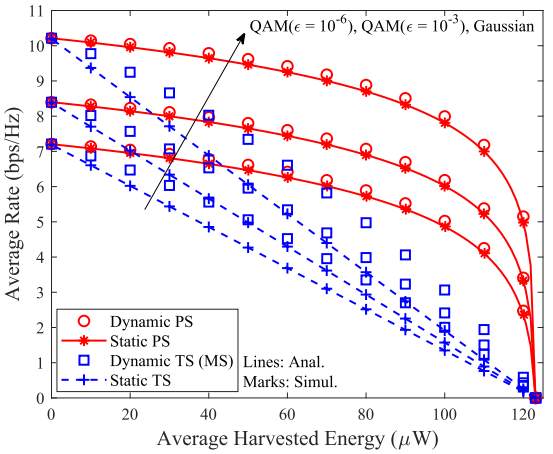

FIGURE 7. Rate-energy regions of the WPBC with different modulations when $d = 5$ m and $M = 4$ for the LEH.

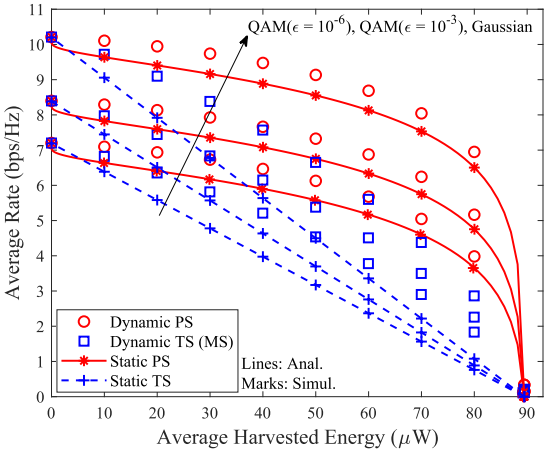

FIGURE 8. Rate-energy regions of the WPBC with different modulations when $d = 5$ m and $M = 4$ for the PLEH.

It should be noted that the dynamic PS provides a gain over the static PS near to the maximum harvesting energy since the dynamic PS in the saturation region can allocate the excess power of the EH to the BM according to the channel state unlike the dynamic TS.

The dynamic PS and MS factors leading to the results of $d = 2$ m and $M = 16$ in Fig. 5 (thus, $E[X] = 2.8 \times 10^{-3}$) are also shown in Fig. 6 for $\mathsf{Q} = 0.1$, 2.0, and 4.4 mW. Again, the optimal dynamic PS factor is given by (45), where $\lambda^{\star}_{P,N}$ and $t^{\star}_{b,2} - t_{w,2}$ increase as Q increases for more EH. The dynamic MS factor is given in the form of $\beta_{M,N}(x|\lambda)$ for $\lambda \geq \lambda_s$ and $N_z = 1$ in Table (1), where $\lambda^{\star}_{M,N}$ increases as Q increases. The rate-energy regions imply that the dynamic PS strategy is more efficient than the dynamic MS (TS) strategy in the saturation region by utilizing the remained power in the EH for the BM.

B. FURTHER INVESTIGATIONS

We investigate the rate-energy regions of the WPBC with practical modulation and EH models and in comparison with the regions of the SWIPT.

Figs. 7 and 8 exhibit the effect of the modulation scheme on the rate-energy regions of the WPBC with the LEH and PLEH, respectively, when $d = 5$ m and $M = 4$. Since a practical modulation scheme reduces the effective SNR γ_0 at the transmitter side and the reduction increases for a higher reliability, the rate performance gets worse by employing the adaptive QAM instead of Gaussian symbols and by decreasing the target BER ϵ for the adaptive QAM.

Fig. 9 compares the rate-energy regions of the WPBC with the static strategies when the PLEH (10) and the SSEH (11) are adopted for the NLEH model of the BD. The regions are evaluated with the BD at $d = 5$ m using Gaussian symbols for $M = 4$ in Fig. 9(a) and $M = 32$ in Fig. 9(b). Note that the regions of the PLEH is obtained with the analysis provided in this paper while the regions of the SSEH is obtained with simulations. The figures show that the analytical results with the PLEH are almost indistinguishable from the simulation results with the SSEH that represents the actual NLEH model.

We also provide the rate-energy regions of the WPBC when the strategies developed with the PLEH are applied to the BD with the SSEH for the actual NLEH model in Fig. 10

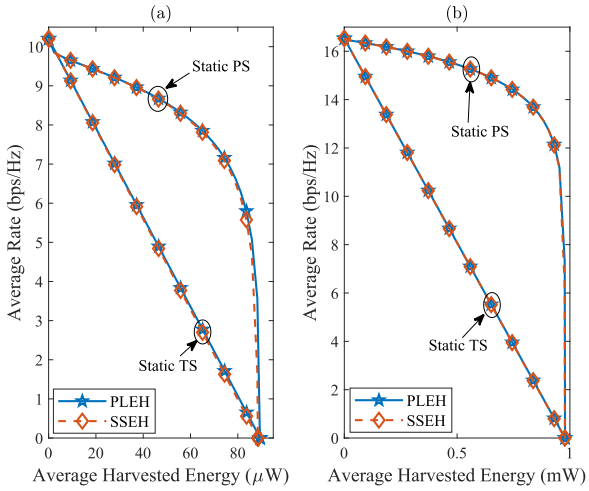

FIGURE 9. Rate-energy regions of the WPBC with the PLEH and the SSEH for the NLEH model of the BD when $d = 5$ m and Gaussian symbols are used: (a) $M = 4$ (b) $M = 32$.

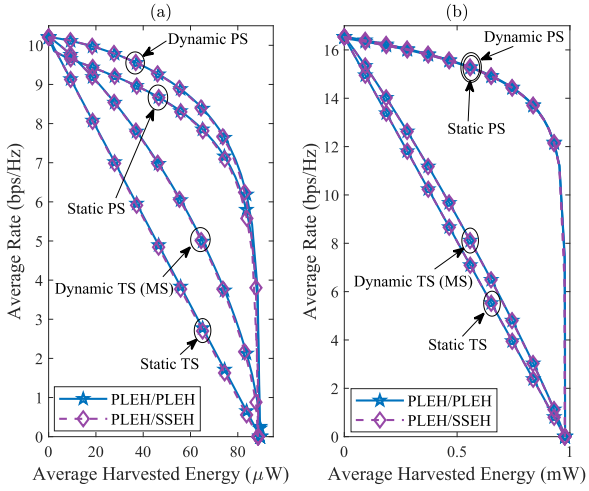

FIGURE 10. Rate-energy regions of the WPBC when the strategies for the PLEH is applied to the BD with the SSEH when $d = 5$ m and Gaussian symbols are used: (a) $M = 4$ (b) $M = 32$.

when the other conditions remain unchanged from Fig. 9. In the figures, PLEH/SSEH denotes the results obtained by applying the strategies derived with the PLEH to the BD with the SSEH while PLEH/PLEH denotes the results obtained in this paper by assuming the PLEH for the NLEH model of the BD. The results show that the rate-energy regions of PLEH/SSEH and PLEH/PLEH coincide each other for the strategy employed. Therefore, it is confirmed that the dynamic PS and TS strategies obtained in explicit forms with the PLEH in this paper are applicable to the BD with the SSEH at a negligible loss.

Finally, we compare the rate-energy regions of the WPBC and SWIPT using Gaussian symbols for BM and the PLEH approximation for the NLEH in Fig. 11 when their device is located at $d = 5$ m. We set $M = 4$ in Fig. 11(a) and $M = 32$ in Fig. 11(b). The energy behaviors are identical for the WPBC and SWIPT since the energy flow is in the same direction from the HAP to the device for both cases.

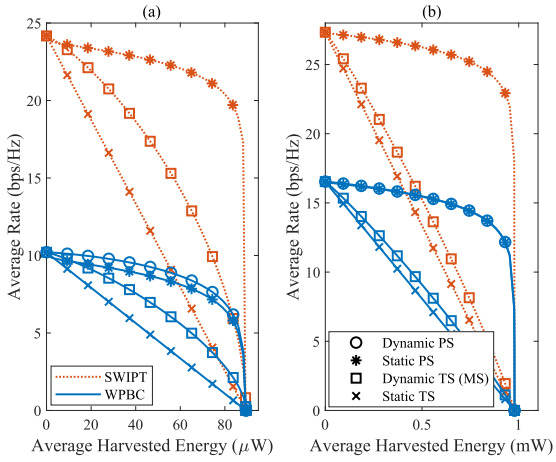

FIGURE 11. Rate-energy regions of the WPBC and SWIPT using Gaussian symbols for BM and the PLEH for the NLEH when $d = 5$ m with (a) $M = 4$ and (b) $M = 32$.

On the other hand, the rate performance of the WPBC is much worse than that of the SWIPT since the WPBC suffers from double path loss and double fading from the HAP to the BD and then from the BD to the HAP while the SWIPT suffers from a single path loss and a single fading from the HAP to the device. The rate gap between the WPBC and SWIPT is reduced by increasing the number of antennas at the HAP which increases the received SNR as well as reduces the double fading effect.

C. DISCUSSIONS

We now discuss some practical implications of the observations made in the preceding subsections. The dynamic PS strategy is the best from a performance perspective in particular with the NLEH models exhibiting a sensitivity region. However, the dynamic PS can be replaced by the static PS to avoid the CSI especially when the number of antennas at the HAP is large. The TS strategies can be employed instead of the PS ones to lower the receiver complexity but at the cost of a considerable performance loss. The rate-energy regions with a practical modulation scheme exhibit a similar shape with those of Gaussian symbols so that the strategies for a practical modulation scheme are obtained immediately from those for Gaussian symbols by adding a SNR margin determined by the reliability condition. The rate-energy regions obtained with the PLEH provide a good approximation to the regions with a practical EH so that the dynamic strategies derived in explicit forms for the PLEH in this paper can be applied to the WPBC with the practical EH. Due to the double path loss and double fading, the rate-energy regions of the WPBC are compressed considerably in comparison with those of the SWIPT. However, the performance gap between the WPBC and SWIPT decreases by increasing the number of antennas at the HAP owing to double beamforming at the transmitter and receiver.

The strategies and their rate-energy regions obtained for the monostatic WPBC with a single BD herein can be applied to the WPBC supporting multiple BDs in a centralized

manner using TDMA and round-robin scheduling. In this case, the rate and energy are reduced according to the portion of a time slot allocated to each BD in the time frame when each BD performs EH and BM in its assigned time slot according to the strategy designed for a single BD. However, the performance of the WPBC with multiple BDs can be improved further by employing sophisticatedly designed strategies and resource allocation methods among the BDs sharing the resources. For instance, even in the aforementioned TDMA, one BD can harvest energy during the time slots allocated for the other BDs, which would change the PS and TS strategies. Furthermore, the rate-energy regions of the WPBC supporting multiple BDs in SDMA can appear in various forms according to the transmit and receive beamforming methods in suppressing the interference as well as how to define the rate-and-energy regions with the rates and energies of multiple BDs. Thus, various optimizations of the multiuser WPBC with PS and TS strategies would be interesting subjects to be tackled as future studies.

VI. CONCLUSION

The rate-energy regions of a monostatic multi-antenna WPBC system were investigated comprehensively with different receiver architectures, the availability of the CSI, and different EH models. The rate-energy regions achieved with the static PS and TS strategies have been analyzed and expressed in closed forms by adopting rate and EH functions reflecting the effect of a practical modulation scheme and a NLEH circuit, respectively. The dynamic PS, MS, and TS strategies have been optimized for each channel state to enlarge the rate-energy region and have been given in closed forms if their optimal dual variable is found, where the dynamic TS strategy is shown to be equivalent to the dynamic MS one. Various investigations show that the rate-energy regions are expanded significantly with the PS strategies rather than the TS (MS) ones at the cost of the receiver complexity, and with the dynamic strategies rather than the static ones at the cost of the CSI. The gain of the dynamic strategies over the static ones is larger with a smaller number of antennas at the HAP or in the sensitivity region of the NLEH while it becomes insignificant with a large number of antennas at the HAP. The results also show that the PS and TS strategies obtained with the PLEH in explicit forms are applicable to the BD with the practical EH model at a negligible loss.

APPENDIX A
PROOFS FOR DYNAMIC PS STRATEGY

A. PROOF OF THEOREM 1

The LEH (9) leads to

$$l_{P,L}(\beta,\lambda,x) = C(\beta\gamma_0\, x^2) + \lambda\{\eta P(1-\beta)x - \mathsf{Q}\} \quad (66)$$

which is a concave function of β. Since the first derivative

$$\frac{\partial}{\partial\beta} l_{P,L}(\beta,\lambda,x) = \frac{\gamma_0\, x^2}{(1+\beta\gamma_0\, x^2)\ln 2} - \lambda\eta P x \quad (67)$$

has a unique zero

$$\beta_z = \frac{1}{\gamma_0\, x^2}\left(\frac{x}{x_0} - 1\right), \quad (68)$$

the right-hand side of (66) has a unique maximum in $\beta \in [0,1]$ which is achieved at $\beta = \beta_z$ if $0 \le \beta_z \le 1$, at $\beta = 0$ if $\beta_z < 0$, and at $\beta = 1$ if $\beta_z > 1$. Hence, we have

$$\beta_{P,L}(x|\lambda) = \begin{cases} 0 & \text{if } x \in \mathfrak{X}_0, \\ \beta_z & \text{if } x \in \mathfrak{X}_z, \\ 1 & \text{if } x \in \mathfrak{X}_1, \end{cases} \quad (69)$$

where

$$\mathfrak{X}_0 = \{\beta_z < 0\} = \{x < x_0\}, \quad (70)$$
$$\mathfrak{X}_z = \{0 \le \beta_z \le 1\} = \{x \ge x_0\} \cap \mathfrak{B}_0, \quad (71)$$
$$\mathfrak{X}_1 = \{\beta_z > 1\} = \{x \ge x_0\} \cap \mathfrak{B}_0^c \quad (72)$$

with $\mathfrak{B}_0$ defined as (40) with φ_0.

If $x_0 < \frac{1}{2\sqrt{\gamma_0}}$ (or equivalently $\lambda < \frac{1}{2}\lambda_{\text{ip}}$), we have $\varphi_0^2 > \frac{4}{\gamma_0}$ and thus $\mathfrak{B}_0 = \{x < t_{0,1} \text{ or } x > t_{0,2}\}$. Since $x_0 < t_{0,1}$ from $t_{0,1} = \frac{1}{\gamma_0 t_{0,2}}$ and $t_{0,2} < \frac{1}{\gamma_0 x_0}$, we have $\mathfrak{X}_z = \{x_0 < x < t_{0,1} \text{ or } x > t_{0,2}\}$ and $\mathfrak{X}_1 = \{t_{0,1} \le x \le t_{0,2}\}$ which lead to (43). If $\lambda \ge \frac{1}{2}\lambda_{\text{ip}}$, $\mathfrak{B}_0 = \mathbb{R}_+$ and $\mathfrak{B}_0^c = \phi$ and thus $\mathfrak{X}_z = \{x \ge x_0\}$ and $\mathfrak{X}_1 = \phi$ which can be obtained by letting $t_{0,1} = t_{0,2} = \infty$ in (43).

B. PROOF OF THEOREM 2

Let us write the objective function (35) for $\mathfrak{h} = N$ as

$$l_{P,N}(\beta,\lambda,x) = \begin{cases} l_{N1}(\beta,\lambda,x) & \text{if } (1-\beta)x \le x_a, \\ l_{N2}(\beta,\lambda,x) & \text{if } x_a < (1-\beta)x < x_b, \\ l_{N3}(\beta,\lambda,x) & \text{if } (1-\beta)x \ge x_b, \end{cases} \quad (73)$$

where

$$l_{N1}(\beta,\lambda,x) = C(\gamma_0\beta x^2) - \lambda\mathsf{Q}, \quad (74)$$
$$l_{N2}(\beta,\lambda,x) = l_{N1}(\beta,\lambda,x) + \lambda\eta P\{(1-\beta)x - x_a\}, \quad (75)$$
$$l_{N3}(\beta,\lambda,x) = C(\gamma_0\beta x^2) + \lambda[P_{sat} - \mathsf{Q}]. \quad (76)$$

Case of $x < x_a$: Since $(1-\beta)x \le x_a$ for $\beta \in [0,1]$, we have $l_{P,N}(\beta,\lambda,x) = l_{N1}(\beta,\lambda,x)$ that is an increasing function of β. Therefore, we have

$$\beta_{P,N}(x|\lambda) = 1 \quad \text{for } x < x_a. \quad (77)$$

Case of $x \ge x_a$: We rewrite (73) as a function of β as

$$l_{P,N}(\beta,\lambda,x) = \begin{cases} l_{N3}(\beta,\lambda,x) & \text{if } 0 \le \beta \le \beta_b^+, \\ l_{N2}(\beta,\lambda,x) & \text{if } \beta_b^+ \le \beta \le \beta_a, \\ l_{N1}(\beta,\lambda,x) & \text{if } \beta_a < \beta \le 1, \end{cases} \quad (78)$$

where $\beta_a = 1 - \frac{x_a}{x}$, $\beta_b = 1 - \frac{x_b}{x}$, and $\beta_b^+ = \max(\beta_b, 0)$. Note that $l_{P,N}(\beta,\lambda,x)$ consists of an increasing function $l_{N3}(\beta,\lambda,x)$, a concave function $l_{N2}(\beta,\lambda,x)$, and an increasing function $l_{N1}(\beta,\lambda,x)$ of β which are continuous at $\beta = \beta_b^+$ and $\beta = \beta_a$. Thus, the maximum of $l_{P,N}(\beta,\lambda,x)$ occurs at one of possible candidates $\{\beta_b^+, \beta_z, 1\}$, where β_z is the zero

of $\frac{\partial}{\partial\beta} l_{N2}(\beta,\lambda,x)=0$; the maximum occurs at either $\beta=\beta_b^+$ or $\beta=1$ if $\beta_z<\beta_b^+$, at either $\beta=\beta_z$ or $\beta=1$ if $\beta_b^+<\beta_z<\beta_a$, and at $\beta=1$ if $\beta_a<\beta_z$. Hence, $\beta_{P,N}(x|\lambda)$ maximizing $l_{P,N}(\beta,\lambda,x)$ is expressed as

$$\beta_{P,N}(x|\lambda)=\begin{cases}\beta_b^+ & \text{if } \beta_z\le\beta_b^+,\\ & l_{N2}(\beta_b^+,\lambda,x)\ge l_{N1}(1,\lambda,x),\\ \beta_z & \text{if } \beta_b^+<\beta_z\le\beta_a,\\ & l_{N2}(\beta_z,\lambda,x)\ge l_{N1}(1,\lambda,x),\\ 1 & \text{otherwise.}\end{cases} \tag{79}$$

We combine (77) and (79) (after replacing $\beta_b^+=0$ for $x_a\le x<x_b$ and $\beta_b^+=\beta_b$ for $x\ge x_b$) into

$$\beta_{P,N}(x|\lambda)=\begin{cases}0 & \text{if } x\in\tilde{\mathfrak{X}}_0,\\ \beta_b & \text{if } x\in\tilde{\mathfrak{X}}_b,\\ \beta_z & \text{if } x\in\tilde{\mathfrak{X}}_z,\\ 1 & \text{otherwise,}\end{cases} \tag{80}$$

where

$$\tilde{\mathfrak{X}}_0=\{x_a\le x<x_b,\ \beta_z\le 0,\ \Delta(0,\lambda,x)\ge 0\}, \tag{81}$$
$$\tilde{\mathfrak{X}}_b=\{x\ge x_b,\ \beta_z\le\beta_b,\ \Delta(\beta_b,\lambda,x)\ge 0\}, \tag{82}$$
$$\tilde{\mathfrak{X}}_z=\{x\ge x_a,\beta_b^+\le\beta_z\}\cap\{\beta_z\le\beta_a,\Delta(\beta_z,\lambda,x)\ge 0\} \tag{83}$$

with

$$\begin{aligned}&\Delta(\beta,\lambda,x)\\ &=l_{N2}(\beta,\lambda,x)-l_{N1}(1,\lambda,x)\\ &=\log_2\left(\frac{1+\gamma_0\beta x^2}{1+\gamma_0 x^2}\right)+\lambda[\eta P\{(1-\beta)x-x_a\}].\end{aligned} \tag{84}$$

In the following, we show that (81)–(83) are equivalent to the expressions in (45).

Case of $\tilde{\mathfrak{X}}_0$: It is straightforward for (81) since $\{\beta_z\le 0\}=\{x\le x_0\}$ and $\Delta(0,\lambda,x)=-D_{N2}(x|\lambda)$.

Case of $\tilde{\mathfrak{X}}_b$: Note that

$$\{\beta_z\le\beta_v\}=\{x^2-\varphi_v x+\frac{1}{\gamma_0}\ge 0\}=\mathfrak{B}_v \tag{85}$$

with $\varphi_v=x_v+\frac{1}{\gamma_0 x_0}$ for $v\in\{a,b\}$ and

$$\{\Delta(\beta_b,\lambda,x)\ge 0\}=\{x^2-\varphi_s x+\frac{1}{\gamma_0}\ge 0\}=\mathfrak{B}_s \tag{86}$$

with $\varphi_s=\frac{x_b}{1-e^{-\lambda P_{sat}}}$. Thus, (82) is rewritten as $\tilde{\mathfrak{X}}_b=\{x\ge x_b\}\cap\mathfrak{B}_b\cap\mathfrak{B}_s$. For $x_b\gg x_a$, we have $\mathfrak{B}_b\cap\mathfrak{B}_s=\mathfrak{B}_b$ since

$$\varphi_b-\varphi_s=\left(1-\frac{1+\varepsilon}{2^{\varepsilon(1-x_a/x_b)}}\right)\frac{1}{\varepsilon(1-e^{-\lambda P_{sat}})}\ge 0 \tag{87}$$

with $\lambda P_{sat}=x_0\gamma_0(x_b-x_a)\ln 2$ and $\varepsilon=x_0\gamma_0 x_b$. Thus, we have

$$\tilde{\mathfrak{X}}_b=\{x\ge x_b\}\cap\mathfrak{B}_b. \tag{88}$$

From $x_b>\frac{2}{\sqrt{\gamma_0}}$, we have $\varphi_b^2>\frac{4}{\gamma_0}$ leading to

$$\mathfrak{B}_b=\{x\le t_{b,1}\text{ or }x\ge t_{b,2}\}, \tag{89}$$

where $t_{b,1}<x_b$ since $t_{b,1}=\frac{1}{\gamma_0 t_{b,2}}<\frac{x_b}{2}$ from $t_{b,2}\ge\frac{x_b}{2}$ and $\frac{4}{\gamma_0}<x_b^2$. Therefore, (88) becomes $\tilde{\mathfrak{X}}_b$ given in (45).

Case of $\tilde{\mathfrak{X}}_z$: We first decompose $\tilde{\mathfrak{X}}_{z1}=\{x\ge x_a,\beta_b^+\le\beta_z\}$ in (83) into

$$\{x\ge x_a,\beta_b<0,\beta_z\ge 0\}\cup\{x\ge x_a,\beta_b\ge 0,\beta_z\ge\beta_b\}, \tag{90}$$

where $\{\beta_b<0\}=\{x<x_b\}$, $\{\beta_z\ge 0\}=\{x\ge x_0\}$, and $\{\beta_z\ge\beta_b\}=\mathfrak{B}_b^c$ from (85). Thus, (90) with (89) becomes

$$\begin{aligned}\tilde{\mathfrak{X}}_{z1}&=\{x_a\le x<x_b,x\ge x_0\}\cup\{x\ge x_b,t_{b,1}\le x\le t_{b,2}\}\\ &=\{\max(x_a,x_0)\le x<\max(x_b,t_{b,2})\}.\end{aligned} \tag{91}$$

Next, we express $\tilde{\mathfrak{X}}_{z2}=\{\beta_z\le\beta_a,\Delta(\beta_z,\lambda,x)\ge 0\}$ in (83) as $\tilde{\mathfrak{X}}_{z2}=\mathfrak{B}_a\cap\mathfrak{D}_z$ from (85), where $\mathfrak{D}_z=\{\Delta(\beta_z,\lambda,x)\ge 0\}$ is rewritten as

$$\mathfrak{D}_z=\{q(x)-\ln q(x)\ge x_0\gamma_0 x_a+1\} \tag{92}$$

with $q(x)=\frac{x_0(1+\gamma_0 x^2)}{x}$. By introducing the Labmert W function, we can express (92) as

$$\begin{aligned}\mathfrak{D}_z&=\{q(x)\le w_0\text{ or }q(x)\ge w_{-1}\}\\ &=\{x^2-\varphi_w x+\frac{1}{\gamma_0}\ge 0\}\cup\{x^2-\varphi_{w'}x+\frac{1}{\gamma_0}\le 0\},\end{aligned} \tag{93}$$

where $w_k=-W_k(-e^{-x_0\gamma_0 x_a-1})$ for $k=-1,0$, $\varphi_w=\frac{w_{-1}}{x_0\gamma_0}$, and $\varphi_{w'}=\frac{w_0}{x_0\gamma_0}$. We further note that

$$\varphi_{w'}\le\varphi_a\le\varphi_w \tag{94}$$

from $w_0\le 1+\gamma_0 x_0 x_a\le w_{-1}$ since $w_0<1$ and $w_{-1}\ge x_0\gamma_0 x_a+1$ from $W_{-1}(-e^{-x})=-x-\ln(W_{-1}(-e^{-x}))\le -x$ for $x\ge 1$. Therefore, we have

$$\tilde{\mathfrak{X}}_{z2}=\mathfrak{D}_z=\{x^2-\varphi_w x+\frac{1}{\gamma_0}\ge 0\}=\mathfrak{B}_w. \tag{95}$$

Thus, the set (83) with (91) and (95) becomes $\tilde{\mathfrak{X}}_z$ in (45).

C. PROOF OF LEMMA 1

If $\lambda<\frac{1}{2}\lambda_{ip}$ (that is, $x_0<\frac{1}{2\sqrt{\gamma_0}}$), we have $\varphi_w^2>\frac{4}{\gamma_0}$ from $\varphi_w\ge\varphi_a=x_a+\frac{1}{x_0\gamma_0}$. Thus, $\mathfrak{B}_w=\{x\le t_{w,1}\text{ or }x\ge t_{w,2}\}$, where $t_{w,2}>x_a$ since $t_{w,2}\ge x_a+\frac{1}{2x_0\gamma_0}>x_a$. Note that $t_{w,1}=\frac{1}{\gamma_0 t_{w,2}}<\frac{1}{\gamma_0 x_a}$ becomes $t_{w,1}<\frac{1}{\sqrt{\gamma_0}}<x_a$ if $x_a>\frac{1}{\sqrt{\gamma_0}}$. If $\lambda<\frac{1}{2}\lambda_{ip}$ and $x_a>\frac{1}{\sqrt{\gamma_0}}$, we have $x_0<x_a$ so that $\tilde{\mathfrak{X}}_0=\phi$, $\tilde{\mathfrak{X}}_z=\{t_{w,2}\le x\le t_{b,2}\}$, and $\tilde{\mathfrak{X}}_b=\{x\ge t_{b,2}\}$.

APPENDIX B
PROOFS FOR DYNAMIC MS STRATEGY

A. PROOF OF THEOREM 3

From (66), (55) is expressed as

$$D_L(x|\lambda)=C(\gamma_0 x^2)-\lambda\eta P x \tag{96}$$

of which the first derivative with respect to x is given by

$$\frac{\partial D_L(x|\lambda)}{\partial x}=-\frac{\lambda\gamma_0\eta P}{1+\gamma_0 x^2}\left(x^2-\frac{2}{x_0\gamma_0}x+\frac{1}{\gamma_0}\right). \tag{97}$$

If $x_0 \geq \frac{1}{\sqrt{\gamma_0}}$, $\frac{\partial D_L(x|\lambda)}{\partial x} \leq 0$ so that $D_L(x|\lambda)$ is decreasing from $D_L(0|\lambda) = 0$ and consequently $D_L(x|\lambda) \leq 0$ for $x \geq 0$. If $x_0 < \frac{1}{\sqrt{\gamma_0}}$, $D_L(x|\lambda)$ is decreasing for $x < t_{L,1}$ or $x > t_{L,2}$ and is increasing for $t_{L,1} < x < t_{L,2}$, where $t_{L,1}$ and $t_{L,2}$ are the two real roots of $\frac{\partial}{\partial x} D_L(x|\lambda) = 0$ expressed as (42) with $q = L$ and $\varphi_L = \frac{2}{x_0\gamma_0}$.

If $D_L(t_{L,2}|\lambda) > 0$, $D_L(x|\lambda)$ has two zeros $z_{L,1}$ and $z_{L,2}$ such that $D_L(x|\lambda) < 0$ for $x < z_{L,1}$ or $x > z_{L,2}$ and $D_L(x|\lambda) > 0$ for $z_{L,1} < x < z_{L,2}$. If $D_L(t_{L,2}|\lambda) \leq 0$, we have $D_L(x|\lambda) \leq 0$ for $x \geq 0$ so that $\beta_{T,L}(x|\lambda) = 0$. The condition $D_L(t_{L,2}|\lambda) > 0$ is equivalent to $x_0 < \sqrt{\frac{\breve{z}}{\gamma_0}}$ and again to $\lambda < \lambda_{\rm ip}\sqrt{\breve{z}}$, where $\breve{z} \approxeq 0.6476$ is the zero of (57) found by the numerical method.

B. PROOF OF THEOREM 4

For the nonlinear PLEH, (55) for $\mathfrak{h} = N$ becomes

$$D_N(x|\lambda) = \begin{cases} C(\gamma_0 x^2) & \text{if } 0 \leq x < x_a, \\ D_{N2}(x|\lambda) & \text{if } x_a \leq x < x_b, \\ D_{N3}(x|\lambda) & \text{if } x \geq x_b, \end{cases} \tag{98}$$

where $D_{N2}(x|\lambda)$ is given in (46) and

$$D_{N3}(x|\lambda) = C(\gamma_0 x^2) - \lambda P_{sat}. \tag{99}$$

Case of $0 \leq x < x_a$: Since $D_N(x|\lambda) > 0$ for all $\lambda > 0$, we have

$$\beta_{M,N}(x|\lambda) = 1 \text{ for } 0 \leq x \leq x_a. \tag{100}$$

Case of $x \geq x_a$: Although $D_{N3}(x|\lambda)$ is an increasing function of $x \in [x_b, \infty)$, $D_{N2}(x|\lambda)$ exhibits a more complicated behavior according to the zeros of $\frac{\partial}{\partial x} D_{N2}(x|\lambda)$, where $\frac{\partial}{\partial x} D_{N2}(x|\lambda) = \frac{\partial}{\partial x} D_L(x|\lambda)$. From (97), $\frac{\partial}{\partial x} D_{N2}(x|\lambda)$ has no zero if $x_0 \geq \frac{1}{\sqrt{\gamma_0}}$ (that is, $\lambda \geq \lambda_{\rm ip}$) while it has two zeros $t_{L,1}$ and $t_{L,2}$ if $\lambda < \lambda_{\rm ip}$.

If $\lambda \geq \lambda_{\rm ip}$, $D_{N2}(x|\lambda)$ is a decreasing function for $x_a \leq x < x_b$ with $D_{N2}(x_a|\lambda) > 0$ while $D_{N3}(x|\lambda)$ is an increasing function for $x > x_b$. Hence, we have a non-trivial solution resulting in $\bar{Q}_{T,N|\lambda} > 0$ only if $D_{N2}(x_b|\lambda) < 0$ (or equivalently $\lambda > \lambda_s \triangleq \frac{C(\gamma_0 x_b^2)}{P_{sat}}$) as

$$\beta_{M,N}(x|\lambda) = \begin{cases} 1 & \text{if } x_a \leq x < z_{N,1} \text{ or } x > z_S, \\ 0 & \text{if } z_{N,1} \leq x < z_S, \end{cases} \tag{101}$$

where $z_{N,1}$ is the unique zero of $D_{N2}(x|\lambda)$ in $x_a \leq x \leq x_b$ and $z_S = \sqrt{\frac{2^{\lambda P_{sat}} - 1}{\gamma_0}}$ is the zero of $D_{N3}(x|\lambda)$. Since $\lambda_{\rm ip} \gg \lambda_s$ in practical scenarios with a large value of γ_0, the solution is given by (101) if $\lambda > \lambda_{\rm ip}$.

If $\lambda < \lambda_{\rm ip}$, $D_{N2}(x|\lambda)$ is decreasing for $x < t_{L,1}$, increasing for $t_{L,1} \leq x < t_{L,2}$, and decreasing for $x \geq t_{L,2}$ with $D_{N2}(x_a|\lambda) > 0$. Thus, $D_{N2}(x|\lambda)$ can have N_z zeros in $x_a \leq x \leq x_b$, where $N_z \in \{0, 1, 2, 3\}$ varies according to the locations of $t_{L,1}$ and $t_{L,2}$ in $x_a \leq x < x_b$. Let $\{z_{N,i}\}_{i=1}^{N_z}$ denote the zeros of $D_{N2}(x|\lambda)$ in $x_a \leq x \leq x_b$. If $\lambda_s < \lambda < \lambda_{\rm ip}$ in which $D_{N2}(x_b|\lambda) < 0$, we have $N_z = 1$ or 3. The dyanmic MS strategy for $N_z = 1$ is given by (101). The dyanmic MS strategy for $N_z = 3$ is expressed as

$$\beta_{M,N}(x|\lambda) = \begin{cases} 1 & \text{if } x_a \leq x < z_{N,1} \text{ or} \\ & \quad z_{N,2} < x < z_{N,3} \text{ or } x < z_S, \\ 0 & \text{if } z_{N,1} < x < z_{N,2} \text{ or } z_{N,3} < x < z_S \end{cases} \tag{102}$$

since $D_{N2}(x|\lambda) > 0$ for $x_a < x < z_{N,1}$ or $z_{N,2} < x < z_{N,3}$ or $x > z_S$ and $D_{N2}(x|\lambda) < 0$ for $z_{N,1} < x < z_{N,2}$ or $z_{N,3} < x < z_{z_S}$. If $\lambda \leq \lambda_s$ with $D_{N2}(x_b|\lambda) \geq 0$, we have $N_z = 0$ or 2, where $N_z = 0$ is trivial. If $N_z = 2$, $D_{N2}(x|\lambda) > 0$ for $x_a < x < z_{N,1}$, $D_{N2}(x|\lambda) < 0$ for $z_{N,1} < x < z_{N,2}$, $D_{N2}(x|\lambda) > 0$ for $z_{N,2} < x < x_b$, and $D_{N3}(x|\lambda) > 0$ for $x > x_b$. Thus, the TS solution is given by

$$\beta_{M,N}(x|\lambda) = \begin{cases} 1 & \text{if } x_a \leq x < z_{N,1} \text{ or } x > z_{N,2}, \\ 0 & \text{if } z_{N,1} \leq x < z_{N,2}. \end{cases} \tag{103}$$

Finally, we have Table 1 by combining (100) with (101)-(103).

C. PROOF OF LEMMA 2

If $x_a > \frac{1}{\sqrt{\gamma_0}}$, $D_{N2}(x|\lambda)$ is concave in $x_a \leq x < x_b$ with $D_{N2}(x_a|\lambda) > 0$. If $\lambda < \lambda_s$, $D_{N2}(x_b|\lambda) > 0$ leading to a trivial solutions with $\beta_{M,N}(x|\lambda) = 1$. If $\lambda \geq \lambda_s$, $D_{N2}(x_b|\lambda) < 0$ and thus the solution is given in Table 1 with $N_z = 1$.

REFERENCES

[1] D. Niyato, D. I. Kim, M. Maso, and Z. Han, "Wireless powered communication networks: Research directions and technological approaches," *IEEE Wireless Commun.*, vol. 24, no. 6, pp. 88–97, Dec. 2017.
[2] T. D. P. Perera, D. N. K. Jayakody, S. K. Sharma, S. Chatzinotas, and J. Li, "Simultaneous wireless information and power transfer (SWIPT): Recent advances and future challenges," *IEEE Commun. Surveys Tuts.*, vol. 20, no. 1, pp. 264–302, 1st Quart., 2018.
[3] C. Xu, L. Yang, and P. Zhang, "Practical backscatter communication systems for battery-free Internet of Things: A tutorial and survey of recent research," *IEEE Signal Process. Mag.*, vol. 35, no. 5, pp. 16–27, Sep. 2018.
[4] A. Bletsas, P. N. Alevizos, and G. Vougioukas, "The art of signal processing in backscatter radio for &μW (or less) Internet of Things: Intelligent signal processing and backscatter radio enabling batteryless connectivity," *IEEE Signal Process. Mag.*, vol. 35, no. 5, pp. 28–40, Sep. 2018.
[5] C. Boyer and S. Roy, "Coded QAM backscatter modulation for RFID," *IEEE Trans. Commun.*, vol. 60, no. 7, pp. 1925–1934, Jul. 2012.
[6] S. C. Boyer and S. Roy, "Backscatter communication and RFID: Coding, energy, and MIMO analysis," *IEEE Trans. Commun.*, vol. 64, no. 3, pp. 770–785, Mar. 2014.
[7] G. Yang, X. Xu, and Y.-C. Liang, "Resource allocation in NOMA-enhanced backscatter communication networks for wireless powered IoT," *IEEE Wireless Commun. Lett.*, vol. 9, no. 1, pp. 117–120, Jan. 2020.
[8] B. Clerckx, Z. Bayani Zawawi, and K. Huang, "Wirelessly powered backscatter communications: Waveform design and SNR-energy tradeoff," *IEEE Commun. Lett.*, vol. 21, no. 10, pp. 2234–2237, Oct. 2017.
[9] C. Yang, X. Wang, and K.-W. Chin, "On max–min throughput in backscatter-assisted wirelessly powered IoT," *IEEE Internet Things J.*, vol. 7, no. 1, pp. 137–147, Jan. 2020.
[10] B. Lyu, D. T. Hoang, and Z. Yang, "Backscatter then forward: A relaying scheme for batteryless IoT networks," *IEEE Wireless Commun. Lett.*, vol. 9, no. 4, pp. 562–566, Apr. 2020.
[11] K. Han and K. Huang, "Wirelessly powered backscatter communication networks: Modeling, coverage, and capacity," *IEEE Trans. Wireless Commun.*, vol. 16, no. 4, pp. 2548–2561, Apr. 2017.
[12] G. Wang, F. Gao, R. Fan, and C. Tellambura, "Ambient backscatter communication systems: Detection and performance analysis," *IEEE Trans. Commun.*, vol. 64, no. 11, pp. 4836–4846, Nov. 2016.

[13] D. Darsena, G. Gelli, and F. Verde, "Modeling and performance analysis of wireless networks with ambient backscatter devices," *IEEE Trans. Commun.*, vol. 65, no. 4, pp. 1797–1814, Apr. 2017.
[14] S. H. Kim and D. I. Kim, "Hybrid backscatter communication for wireless-powered heterogeneous networks," *IEEE Trans. Wireless Commun.*, vol. 16, no. 10, pp. 6557–6570, Oct. 2017.
[15] W. Zhao, G. Wang, R. Fan, L.-S. Fan, and S. Atapattu, "Ambient backscatter communication systems: Capacity and outage performance analysis," *IEEE Access*, vol. 6, pp. 22695–22704, 2018.
[16] Q. Zhang, L. Zhang, Y.-C. Liang, and P.-Y. Kam, "Backscatter-NOMA: A symbiotic system of cellular and Internet-of-Things networks," *IEEE Access*, vol. 7, pp. 20000–20013, 2019.
[17] D. Darsena, G. Gelli, and F. Verde, "Cloud-aided cognitive ambient backscatter wireless sensor networks," *IEEE Access*, vol. 7, pp. 57399–57414, 2019.
[18] Y. Liao, G. Yang, and Y.-C. Liang, "Resource allocation in NOMA-enhanced full-duplex symbiotic radio networks," *IEEE Access*, vol. 8, pp. 22709–22720, 2020.
[19] G. Yang, C. K. Ho, and Y. L. Guan, "Multi-antenna wireless energy transfer for backscatter communication systems," *IEEE J. Sel. Areas Commun.*, vol. 33, no. 12, pp. 2974–2987, Dec. 2015.
[20] I. Krikidis, "Retrodirective large antenna energy beamforming in backscatter multi-user networks," *IEEE Wireless Commun. Lett.*, vol. 7, no. 4, pp. 6780–681, Aug. 2018.
[21] J. C. Kwan and A. O. Fapojuwo, "Sum-throughput maximization in wireless sensor networks with radio frequency energy harvesting and backscatter communication," *IEEE Sensors J.*, vol. 18, no. 17, pp. 7325–7339, Sep. 2018.
[22] Z. B. Zawawi, Y. Huang, and B. Clerckx, "Multiuser wirelessly powered backscatter communications: Nonlinearity, waveform design, and SINR-energy tradeoff," *IEEE Trans. Wireless Commun.*, vol. 18, no. 1, pp. 241–253, Jan. 2019.
[23] D. Mishra and E. G. Larsson, "Optimal channel estimation for reciprocity-based backscattering with a full-duplex MIMO reader," *IEEE Trans. Signal Process.*, vol. 67, no. 6, pp. 1662–1677, Mar. 2019.
[24] D. Mishra and E. G. Larsson, "Sum throughput maximization in multi-tag backscattering to multiantenna reader," *IEEE Trans. Commun.*, vol. 67, no. 8, pp. 5689–5705, Aug. 2019.
[25] D. Mishra and E. G. Larsson, "Multi-tag backscattering to MIMO reader: Channel estimation and throughput fairness," *IEEE Trans. Wireless Commun.*, vol. 18, no. 12, pp. 5584–5599, Dec. 2019.
[26] C. He, S. Chen, H. Luan, X. Chen, and Z. J. Wang, "Monostatic MIMO backscatter communications," *IEEE J. Sel. Areas Commun.*, vol. 38, no. 8, pp. 1896–1909, Aug. 2020.
[27] L. Liu, R. Zhang, and K.-C. Chua, "Wireless information transfer with opportunistic energy harvesting," *IEEE Trans. Wireless Commun.*, vol. 12, no. 1, pp. 288–300, Jan. 2013.
[28] L. Liu, R. Zhang, and K.-C. Chua, "Wireless information and power transfer: A dynamic power splitting approach," *IEEE Trans. Commun.*, vol. 61, no. 9, pp. 3990–4001, Sep. 2013.
[29] X. Zhou, R. Zhang, and C. K. Ho, "Wireless information and power transfer: Architecture design and rate-energy tradeoff," *IEEE Trans. Commun.*, vol. 61, no. 11, pp. 4754–4767, Nov. 2013.
[30] J.-M. Kang, I.-M. Kim, and D. I. Kim, "Mode switching for SWIPT over fading channel with nonlinear energy harvesting," *IEEE Wireless Commun. Lett.*, vol. 6, no. 5, pp. 678–681, Oct. 2017.
[31] J.-M. Kang, I.-M. Kim, and D. I. Kim, "Joint optimal mode switching and power adaptation for nonlinear energy harvesting SWIPT system over fading channel," *IEEE Trans. Commun.*, vol. 66, no. 4, pp. 1817–1832, Apr. 2018.
[32] B. Clerckx, R. Zhang, R. Schober, D. W. K. Ng, D. I. Kim, and H. V. Poor, "Fundamentals of wireless information and power transfer: From RF energy harvester models to signal and system designs," *IEEE J. Sel. Areas Commun.*, vol. 37, no. 1, pp. 4–33, Jan. 2019.
[33] J.-M. Kang, C.-J. Chun, I.-M. Kim, and D. I. Kim, "Dynamic power splitting for SWIPT with nonlinear energy harvesting in ergodic fading channel," *IEEE Internet Things J.*, vol. 7, no. 6, pp. 5648–5665, Jun. 2020.
[34] S. Wang, M. Xia, K. Huang, and Y.-C. Wu, "Wirelessly powered two-way communication with nonlinear energy harvesting model: Rate regions under fixed and mobile relay," *IEEE Trans. Wireless Commun.*, vol. 16, no. 12, pp. 8190–8204, Dec. 2017.
[35] P. N. Alevizos and A. Bletsas, "Sensitive and nonlinear far-field RF energy harvesting in wireless communications," *IEEE Trans. Wireless Commun.*, vol. 17, no. 6, pp. 3670–3685, Jun. 2018.
[36] L. Cantos and Y. H. Kim, "Max-min fair energy beamforming for wireless powered communication with non-linear energy harvesting," *IEEE Access*, vol. 7, pp. 69516–69523, 2019.
[37] S. J. Thomas, E. Wheeler, J. Teizer, and M. S. Reynolds, "Quadrature amplitude modulated backscatter in passive and semipassive UHF RFID systems," *IEEE Trans. Microw. Theory Techn.*, vol. 60, no. 4, pp. 1175–1182, Apr. 2012.
[38] R. Correia, A. Boaventura, and N. B. Carvalho, "Quadrature amplitude backscatter modulator for passive wireless sensors in IoT applications," *IEEE Trans. Microw. Theory Techn.*, vol. 65, no. 4, pp. 1103–1110, Apr. 2017.
[39] X. Hao, H. Zhang, Z. Shen, Z. Liu, L. Zhang, H. Jiang, J. Liu, and H. Liao, "A 43.2 μW 2.4 GHz 64-QAM pseudo-backscatter modulator based on integrated directional coupler," in *Proc. IEEE Int. Symp. Circuits Syst. (ISCAS)*, May 2018, pp. 1–5.
[40] A. Goldsmith, *Wireless Communications*. Cambridge, U.K.: Cambridge Univ. Press, 2005.
[41] J. Choi, *Optimal Combining and Detection: Statistical Signal Processing for Communications*. Cambridge, U.K.: Cambridge Univ. Press, 2010.
[42] I. S. Gradshteyn and I. M. Ryzhik, *Table of Integrals, Series, and Products*, 7th ed. New York, NY, USA: Academic, 2007.
[43] A. P. Prudnikov, Y. A. Brychkov, and O. I. Marichev, *Table of Integrals, Series, and Products*, vol. 3. New York, NY, USA: Gordon and Breach Science Publishers, 1990.
[44] W. Yu and R. Lui, "Dual methods for nonconvex spectrum optimization of multicarrier systems," *IEEE Trans. Commun.*, vol. 54, no. 7, pp. 1310–1322, Jul. 2006.
[45] S. Boyd and L. Vandenberghe, *Convex Optimization*. Cambridge, U.K.: Cambridge Univ. Press, 2004.
[46] I. Chatzigeorgiou, "Bounds on the lambert function and their application to the outage analysis of user cooperation," *IEEE Commun. Lett.*, vol. 17, no. 8, pp. 1505–1508, Aug. 2013.

GERARDO SACARELO received the B.S.E. degree in electronics and telecommunications engineering from the Escuela Superior Politécnica del Litoral (ESPOL), Ecuador, in 2014. He is currently pursuing the combined M.S. and Ph.D. degree in electronic engineering with Kyung Hee University, South Korea. His research interests include cooperation communication, massive MIMO, and wireless powered communication with energy harvesting.

YUN HEE KIM (Senior Member, IEEE) received the B.S.E. *(summa cum laude)*, M.S.E., and Ph.D. degrees in electrical engineering from the Korea Advanced Institute of Science and Technology, Daejeon, South Korea, in 1995, 1997, and 2000, respectively. From 2000 to 2011, she was with the Department of Electrical and Computer Engineering, University of California at San Diego, La Jolla, CA, USA, as a Visiting Researcher. From September 2000 to August 2004, she was a Senior Member of Research Staff with the Electronics and Telecommunications Research Institute, Daejeon. In September 2004, she joined the Department of Electronic Engineering, Kyung Hee University, Yongin, South Korea, where she is currently a Professor. Her research interests include wireless/mobile communications, statistical signal processing, and the ultra-low power Internet-of-Things.